



Universidade Federal
do Rio de Janeiro

Escola Politécnica

DATA ANALYSIS OF THE DYNAMIC BEHAVIOR IN INTERFACIAL TENSION MEASUREMENTS BETWEEN CRUDE OIL AND BRINE

Elton Lima Correia

Projeto de Graduação submetido ao Corpo Docente do Curso de Engenharia de Petróleo da Escola Politécnica da Universidade Federal do Rio de Janeiro como parte integrante dos requisitos necessários à obtenção do título de Engenheiro de Petróleo.

Orientadores: Prof. Santiago Gabriel Drexler, D. Sc.

Prof. Paulo Couto, D. Eng.

Rio de Janeiro

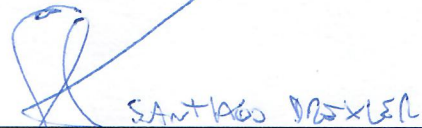
May 2019

**DATA ANALYSIS OF THE DYNAMIC BEHAVIOR IN
INTERFACIAL TENSION MEASUREMENTS BETWEEN CRUDE
OIL AND BRINE**

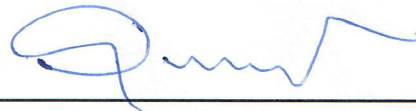
Elton Lima Correia

PROJETO DE GRADUAÇÃO SUBMETIDO AO CORPO DOCENTE DO CURSO DE ENGENHARIA DE PETRÓLEO DA ESCOLA POLITÉCNICA DA UNIVERSIDADE FEDERAL DO RIO DE JANEIRO COMO PARTE INTEGRANTE DOS REQUISITOS NECESSÁRIOS À OBTENÇÃO DO TÍTULO DE ENGENHEIRO DE PETRÓLEO.

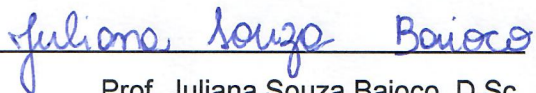
Examinado por:



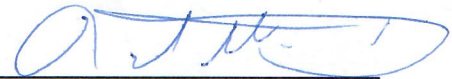
Prof. Santiago Gabriel Drexler, D.Sc.



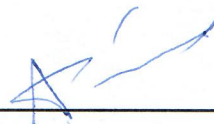
Prof. Paulo Couto, D.Eng.



Prof. Juliana Souza Baioco, D.Sc.



Prof. Rafael Mengotti Charin, D.Sc.



Prof. Aurora Perez Gramatges, Ph.D.

Rio de Janeiro

May 2019

Lima Correia, Elton

Data analysis of the dynamic behavior in interfacial tension measurements between crude oil and brine / Elton Lima Correia – Rio de Janeiro: UFRJ / Escola Politécnica, 2019.

XIII, 68p.:il.; 29,7cm.

Orientadores: Santiago Gabriel Drexler e Paulo Couto
Projeto de Graduação – UFRJ / Escola Politécnica / Engenharia de Petróleo, 2019.

Referências Bibliográficas: p. 53-55.

1. Interfacial Tension. 2. Enhanced Oil Recovery. 3. Brazilian Pre-salt. 4. DSA.

I. Drexler, Santiago Gabriel & Couto, Paulo. II. Universidade Federal do Rio de Janeiro, Escola Politécnica, Curso de Engenharia de Petróleo. III. Data analysis of the dynamic behavior in interfacial tension measurements between crude oil and brine.

Dedico este trabalho aos meus pais, que não mediram esforços para possibilitar a minha formação.

Acknowledgements

Agradeço primeiramente a minha mãe, Maria Josileide de Lima, e ao meu pai, Juarez Gomes Correia. Vocês me deram a oportunidade de viver, e ficaram ao meu lado desde então. Me deram forças para superar todas as dificuldades que a vida apresenta e continuam fazendo isso. Espero que um dia eu consiga retribuir um pouco do que vocês proporcionaram durante toda minha vida.

Gostaria também de agradecer a pessoa mais importante na minha vida há quase 5 anos. Ana Carolina Roncoli Jerdy, você tem sido minha amiga, companheira, namorada, exemplo e inspiração da minha vida durante esses anos juntos. Não existem palavras para descrever o quão agradecido eu sou por ter você na minha vida, me apoiando em tudo que eu faço. Eu só sou o que sou hoje por sua culpa, obrigado por tudo, meu amor.

Agradeço ao meu orientador Prof. D. Sc. Santiago Gabriel Drexler. Você acreditou em meu potencial e me deu oportunidades únicas em pouco mais de 2 anos. Suas aulas me ensinaram a pensar do jeito que penso hoje. Você me ensinou a resolver problemas. Você mudou a minha vida, professor! Farei tudo que puder para honrar a confiança que você depositou em mim.

Gostaria de agradecer também ao Prof. D. Eng. Paulo Couto, por todas as aulas e conhecimento passado durante a minha caminhada na universidade. Suas aulas foram onde me apaixonei por essa indústria cheia de desafios.

Também gostaria de agradecer a todos os professores que aceitaram fazer parte da minha banca avaliadora, Prof. D.Sc. Juliana Souza Baioco, Prof. D.Sc. Rafael Mengotti Charin e Prof. Ph.D. Aurora Perez Gramatges. Sou muito grato pelo que já aprendi com cada um de vocês.

Tenho que agradecer a todos companheiros do PetroTeam UFRJ que fizeram parte da minha caminhada. Vocês, Ana Jerdy, Felipe Adrião, Felipe Pardini, Gabriel Costa, Felipe Pontual, Velemu Lubisse, Marco Tulio e claro, Santiago Drexler, me proporcionaram momentos inesquecíveis e contribuíram muito para o rumo que minha vida tomou. Esse time abriu as portas do mundo para mim. Juntos conquistamos a América do Sul e Caribe duas vezes. Mais do que companheiros de time, vocês se tornaram amigos. Muito obrigado!

Impossível não falar de quem esteve comigo desde o início dessa faculdade. Ronie Fiuza, Alexandre Lima, Lucas Fernandes e Júlia Lourenço, vocês são os irmãos

que eu escolhi. Rimos juntos, sofremos juntos e bebemos juntos. Muito obrigado por todas as vezes que vocês “quebraram árvores” para mim. Muito obrigado por serem um dos motivos de vir à faculdade durante esses 5 anos. Saibam que não há Elton sem vocês.

Gostaria também de agradecer amigos que estiveram comigo durante parte da minha vida, e deixaram sua marca. Victor Elias, Kalyel Sousa, Matheus Rodrigues, Alan Neumann, Gabryel Henrique, Rodrigo Siqueira, Gabriel Damasceno, Rafael Rodrigues, Kayro Aguillar, Rafael Bonani, André Gomes, Gabriel de Belli, Mariana Frias e Raíssa Yabiko. Muito obrigado, vocês foram importantes de alguma forma durante minha vida!

Gostaria de agradecer ao Laboratório de Recuperação Avançada de Petróleo (LRAP), que me proporcionou experiências inéditas que eu jamais imaginaria. Um agradecimento especial à M. Sc. Thaís Márcia, mulher guerreira, gente boa e mais animada que eu conheço. Você fez o possível e o impossível para me ajudar. Muito obrigado, de coração. Você é a melhor de todas!

Não posso esquecer de alguns professores, que também marcaram minha vida e me ensinaram coisas que aplico até hoje ao meu cotidiano. Fábio Capella, Andréa Cristina, Eugênio Azevedo, Heraldo Filho, Marcelo Mendes, Jorge Rodrigues e Rosemarie Bone. Muito obrigado, mestres!

Finalmente, gostaria de agradecer à UFRJ, instituição que aprendi a amar nestes últimos anos. Foi muito bom fazer parte da melhor escola de engenharia de petróleo do Brasil. Foi muito bom representar a segunda maior universidade do país pelo Brasil e pelo mundo. Foi uma honra ser um filho da Minerva!

Resumo do Projeto de Graduação apresentado à Escola Politécnica/UFRJ como parte dos requisitos necessários para a obtenção do grau de Engenheiro de Petróleo.

ANÁLISE DE DADOS DO COMPORTAMENTO DINÂMICO EM MEDIDAS DE TENSÃO INTERFACIAL ENTRE ÓLEO CRU E SALMOURA

Elton Lima Correia

Maio de 2019

Orientador: Prof. Santiago Gabriel Drexler, D. Sc.

Orientador: Prof. Paulo Couto, D. Eng.

Curso: Engenharia de Petróleo

Métodos de recuperação avançada de petróleo têm sido utilizados ao longo da história da indústria petrolífera com o objetivo de aumentar o volume de óleo recuperado do reservatório. Entre eles, os métodos miscíveis que utilizam a injeção de CO₂ são aplicados nos reservatórios do Pré-sal brasileiro, tanto para aumentar o fator de recuperação quanto para o armazenamento de dióxido de carbono. Acredita-se que este método tenha um impacto na tensão interfacial entre os fluidos do reservatório *in situ*. Neste trabalho vários experimentos contendo diferentes fases e uma composição constante de salmoura foram analisados. Pressões variando de 1000 psi a 5000 psi e temperatura de 60 °C foram as condições. Este trabalho propõe um método de extrapolação de medidas de tensão interfacial usando uma aproximação logarítmica. Vários sistemas são analisados para que seja possível perceber como esse método se ajusta a diferentes cenários. Esta extrapolação pode ser útil para determinar valores estáveis de tensão interfacial com testes de períodos curtos. Os valores de R² foram, em média, maiores que 0,9. Foi possível concluir que essa aproximação é boa, mostrando que poucas horas de medição são suficientes para inferir o valor que a tensão interfacial se aproximaria em longos períodos. Foi possível perceber que a adição de CO₂ aos fluidos reduziu consideravelmente o tempo de estabilização quando comparado com as mesmas medidas sem CO₂. Além disso, a presença de componentes ativos de superfície nas análises de óleo cru mostrou que eles têm um papel importante na redução do valor final da tensão interfacial.

Palavras-chave: Tensão Interfacial, Recuperação Avançada de Petróleo, Pré-Sal Brasileiro, DSA

Abstract of the Undergraduate Project presented to POLI/UFRJ as partial fulfillment of the requirements for the degree of Petroleum Engineer.

DATA ANALYSIS OF THE DYNAMIC BEHAVIOR IN INTERFACIAL TENSION MEASUREMENTS BETWEEN CRUDE OIL AND BRINE

Elton Lima Correia

May/2019

Advisor: Prof. Santiago Gabriel Drexler, Dr. Sc.

Advisor: Prof. Paulo Couto, Dr. Eng.

Major: Petroleum Engineering

Enhanced Oil Recovery methods have been used throughout the history of the oil industry aiming to increase the volume of oil recovered from the reservoir. Among these methods, miscible methods utilizing CO₂ injection are employed in Brazilian Pre-salt reservoirs for both increasing the recovery factor and carbon dioxide storage. This method is believed to have an impact on interfacial tension between reservoir fluids *in situ*. In this work, several experiments with different oil phases and a constant brine composition were analysed. Pressure were varied from 1000 psi to 5000 psi and temperature was 60 °C. This work proposes a method of extrapolating interfacial tension measurements using a logarithmic approximation. Several systems are analysed so it is possible to notice how this method fits different scenarios. This extrapolation can be useful to determine stable values of interfacial tension with short period tests. The R² values were on average greater than 0,9. It was possible to conclude that this approximation is good, showing that with few hours of measurement are enough to infer the value that interfacial tension would approach at long periods. It was possible to notice that the CO₂ addition to the fluids considerably diminished the stabilization time when compared to the same measurements without CO₂. Futhermore, the presence of surface-active components in the crude oil analysed showed that they have a major role in reducing the final value of interfacial tension.

Keywords: Interfacial Tension, Enhanced Oil Recovery, Brazilian Pre-Salt, DSA

Table of Contents

| | |
|--|------|
| LIST OF FIGURES | xi |
| LIST OF TABLES | xiii |
| CHAPTER 1: INTRODUCTION | 1 |
| 1.1 Motivations and Goals | 1 |
| 1.2 Structure..... | 4 |
| CHAPTER 2: LITERATURE REVIEW..... | 5 |
| 2.1 Interfacial Tension | 5 |
| 2.1.1 Surface-active agents..... | 9 |
| 2.1.2 CO ₂ | 10 |
| 2.1.3 Density..... | 11 |
| 2.1.4 Pendant drop method..... | 12 |
| 2.1.5 Dynamic behavior | 14 |
| 2.2 Data analysis | 15 |
| 2.2.1 Curve fitting | 15 |
| 2.2.2 Gaussian distribution | 16 |
| 2.2.3 Coefficient of determination | 17 |
| CHAPTER 3: MATERIALS AND METHODS | 18 |
| 3.1 Materials..... | 18 |
| 3.2 Materials characterization..... | 18 |
| 3.2.1 Brine B | 18 |
| 3.2.2 Model Oil I | 19 |
| 3.2.3 Model Oil II | 20 |
| 3.2.4 Oil B | 20 |
| 3.3 Samples preparation..... | 21 |
| 3.3.1 Formation Water..... | 21 |
| 3.3.2 Model oil II..... | 21 |

| | |
|--|----|
| 3.3.3 CO ₂ dissolution in fluids..... | 22 |
| 3.4 Density determination | 22 |
| 3.5 Pendant drop experiment..... | 22 |
| 3.6 Data analysis | 24 |
| 3.6.1 Stabilization time | 27 |
| CHAPTER 4: RESULTS AND DISCUSSIONS | 28 |
| 4.1 Curve fitting | 28 |
| 4.1.1 Method validation | 28 |
| 4.1.2 Fluids without CO ₂ | 30 |
| 4.1.2.1 Model oil I | 30 |
| 4.1.2.2 Model Oil II | 32 |
| 4.1.2.3 Oil B | 34 |
| 4.1.3 Fluid with CO ₂ | 35 |
| 4.2 Stabilization time | 37 |
| 4.2.1 Fluids without CO ₂ | 37 |
| 4.2.1.1 Model Oil I | 37 |
| 4.2.1.2 Model Oil II | 39 |
| 4.2.1.3 Oil B | 40 |
| 4.2.2 Fluid with CO ₂ | 42 |
| 4.3 Dynamic IFT x Stable IFT | 44 |
| 4.3.1 Fluids without CO ₂ | 45 |
| 4.3.1.1 Model Oil I | 45 |
| 4.3.1.2 Model Oil II | 46 |
| 4.3.1.3 Oil B | 47 |
| 4.3.2 Fluid with CO ₂ | 48 |
| 4.3.3 Comparison between the systems..... | 48 |
| CHAPTER 5: CONCLUSIONS AND FUTURE WORK..... | 51 |
| BIBLIOGRAPHY | 53 |

LIST OF FIGURES

| | |
|--|----|
| Figure 1 - EOR method based on lithology (MANRIQUE et al., 2010)..... | 2 |
| Figure 2 - Scheme of bulk and interfacial interactions between two molecules (ROSEN; KUNJAPPU, 2012) | 5 |
| Figure 3 - Scheme of phase segregation | 7 |
| Figure 4 - Capillary desaturation curve for a water-wet rock (SHOSA; SCHRAMM, 2001) | 9 |
| Figure 5 - Scheme of SARA classification of crude oil (GUDMUNDSSON, 2017) | 10 |
| Figure 6 - Pendant drop profile (SONG; SPRINGER, 1996)..... | 12 |
| Figure 7 - Empirical rule for normal distributions | 16 |
| Figure 8 - DSA apparatus scheme | 23 |
| Figure 9 - Oil B + Brine B untreated scattered data..... | 24 |
| Figure 10 - Oil B + Brine B smoothed scattered data | 25 |
| Figure 11 - Oil B + Brine B fitting function with equation and R ² | 25 |
| Figure 12 - Oil B + Brine B first five hours of measurement..... | 26 |
| Figure 13 - Plot of a negative logarithmic function | 27 |
| Figure 14 - Hexane and water at atmospheric pressure and 27 °C | 28 |
| Figure 15 - Hexane + water at atmospheric pressure and 50 °C | 29 |
| Figure 16 - Model oil I x Brine B at 1000 psi..... | 30 |
| Figure 17 - Model oil I x Brine B at 5000 psi..... | 31 |
| Figure 18 - Model oil II x Brine B at 1000 psi..... | 33 |
| Figure 19 - Model oil II x Brine B at 5000 psi..... | 33 |
| Figure 20 - Oil B x Brine B at 1000 psi | 34 |
| Figure 21 - Model Oil II x Brine B with CO ₂ at 1000 psi | 36 |
| Figure 22 - Model Oil II x Brine B with CO ₂ at 5000 psi | 36 |
| Figure 23 - Stabilization time of Model Oil I with different thresholds..... | 37 |
| Figure 24 - Model Oil I IFT values for different thresholds | 38 |
| Figure 25 - Semilog plot of model oil I IFT..... | 38 |
| Figure 26 - Stabilization time of Model Oil II with different thresholds..... | 39 |
| Figure 27 - Model Oil II IFT values for different thresholds..... | 39 |
| Figure 28 - Semilog plot of model oil II IFT..... | 40 |
| Figure 29 - Stabilization time of Oil B with different thresholds..... | 40 |
| Figure 30 - Oil B IFT values for different thresholds | 41 |
| Figure 31 - Semilog plot of Oil B IFT | 42 |
| Figure 32 - Stabilization time of Model oil II + CO ₂ with different thresholds | 42 |

| | |
|--|----|
| Figure 33 – Model Oil II + CO ₂ IFT values for different thresholds..... | 43 |
| Figure 34 - Semilog plot of Model oil II with CO ₂ IFT | 44 |
| Figure 35 - Time lapse of drop phase (Oil B x Brine B at 5000 psi) | 44 |
| Figure 36 - Model Oil I IFT comparison..... | 45 |
| Figure 37 - Model Oil II IFT comparison | 46 |
| Figure 38 - Oil B IFT comparison | 47 |
| Figure 39 - Model Oil II + CO ₂ IFT comparison | 48 |
| Figure 40 - IFT comparison without CO ₂ | 48 |
| Figure 41 - Density difference between brine and oily phases | 49 |
| Figure 42 - IFT comparison between Model Oil II with and without CO ₂ | 50 |

LIST OF TABLES

| | |
|--|----|
| Table 1 - Ionic composition of brine B (DREXLER et al., 2019)..... | 19 |
| Table 2 - Brine B density..... | 19 |
| Table 3 - Model Oil I density | 20 |
| Table 4 - Model Oil II densities..... | 20 |
| Table 5 - Oil B SARA analysis | 20 |
| Table 6 - Oil B density..... | 21 |
| Table 7 - Comparison between measured and calculated IFT | 26 |
| Table 8 - Comparison between literature and caculated data..... | 29 |
| Table 9 - Equation coefficients for model oil I at 1000 psi | 30 |
| Table 10 - Range of reliable values for coefficients of model oil I at 1000 psi..... | 31 |
| Table 11 - Equation coefficients for model oil I at 5000 psi | 31 |
| Table 12 - Average values and reliable limit considering 6 th measurement for model oil I 5000 psi..... | 32 |
| Table 13 - Average values and reliable limit without considering 6 th measurement for model oil I at 5000 psi..... | 32 |
| Table 14 - Equation coefficients for oil B at 1000 psi..... | 34 |
| Table 15 - Oil B coefficients for all pressures | 35 |

CHAPTER 1: INTRODUCTION

1.1 Motivations and Goals

The rise of the global oil demand along with the exploration of mature fields and already known reserves is turning the industry to improve the yield of oil and gas fields. The recovery factor is a measure of how well a reservoir was explored. It is defined as the ratio between the cumulative production and the original oil in place (OOIP). Among several means of achieving a higher Recovery Factor (RF), the Enhanced Oil Recovery (EOR) methods are under the spotlight (MANRIQUE et al., 2010).

Traditionally, such methods are called “tertiary recovery methods”. These are applied at the end of the life of the oil field, aiming to improve the oil production after the primary and secondary recovery methods. Primary methods are reservoir natural forces that drive the oil to the production facility by itself, which are gas drive, water drive and compaction drive. The secondary recovery methods are interventions on the field that are made to prolong its life by means of maintaining the reservoir pressure at a desired level and sweeping the oil from the pores. Examples are water and gas flooding.

The EOR methods can be divided into subcategories: Chemical, Thermal, Miscible, Microbiological and Nanotechnological. Each of them has a different mechanism for improving the recovery factor and is suitable for different scenarios. Figure 1 shows a survey of 1507 projects classified according to the EOR method and lithology. In the Brazilian Pre-salt carbonate rocks, the miscible methods are considered the most suitable ones. These reservoirs have a high production of CO₂, which cannot be vented due to environmental concerns. In addition, the production platforms are kilometers distant from continental shelf (PIZARRO et al., 2017). In this method, a gas (usually CO₂ or CO₂ enriched natural gas) is injected into the reservoir to be mixed with the oil *in situ* and to generate a lighter product, which has a lower viscosity and flows easier through the pores. There are also other effects involved in this mixture, like the swelling of oil, and the reduction of interfacial tension between the oil and the formation water (GOZALPOUR; REN; TOHIDI, 2005).

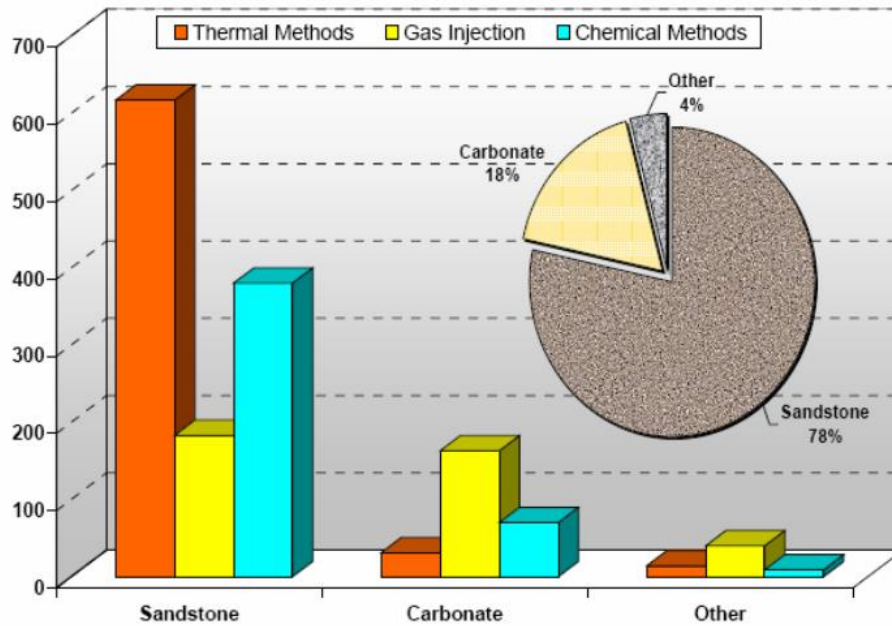


Figure 1 - EOR method based on lithology (MANRIQUE et al., 2010)

Two efficiencies which are involved in the production of an oil reservoir that have a great influence on the resulting RF:

- The sweep or macroscopic efficiency, that shows how well a reservoir was swept by the injected fluid during the secondary recovery period, vertically and areally;
- The displacement efficiency, or microscopic efficiency, that is related to phenomena at the pore scale such as capillarity and wettability.

The RF can also be defined as the product of both these efficiencies (SHENG, 2010).

Thus, to maximize the RF, one needs to maximize both sweep and displacement efficiencies. Macroscopic efficiency is achieved with conformance control by choosing an adequate fluid aiming a mobility ratio below 1. In contrast, microscopic efficiency depends on rock and fluid properties that are more difficult to be changed, as this efficiency is related to the wettability and the interfacial tension (IFT) between the oil and water in the formation (SHENG, 2010). If the rock is oil-wet and the IFT between the reservoir fluids is high, the capillary pressure to displace this fluid from the small pores could be extremely high, making it impossible to recover the oil. Hence, IFT is of paramount importance because it affects directly the displacement efficiency, which in turn affects the RF.

Several experimental techniques were developed to measure the IFT between oil and water. The Drop Shape Analyser (DSA) is used to carry in pendant drop experiments, with the sample subjected to hostile environments such as high pressure

and high temperature (HPHT). This kind of test can be used to emulate the reservoir condition, obtaining more realistic measurements.

Data analysis is of paramount importance to interpret data correctly. Without adequate data analysis, the data collected in tedious experimental tests are of no value. IFT experiments are time dependent, i.e. the values measured at early times are usually higher than the ones taken later (ROSEN; KUNJAPPU, 2012). This dynamic behavior introduces complexity to the data analysis. Therefore, to analyse better the data set, a methodology must be developed in order to acquire consistent results.

In some experiments, points are acquired at previously determined sampling rates, leading to a discrete data set. Due to this, the measured property is not represented continuously. Interpolations between measured points must be done in order to acquire values that do not match the discrete domain generated by the experiment. This is accomplished by the use of algebraic functions which can be used to represent the trend of the data set.

This work proposes the use of a logarithmic function to model the time dependence of IFT. As a way to ensure the representativeness of the fitting function to the actual data points, the R^2 value is analysed. The R^2 (or coefficient of determination) is the proportion of the variance in the dependent variable that is predictable from the independent variable, or variables.

Given the dynamic behavior of IFT, two possible situations can be modeled using measurements from different periods. First, during a fluid flooding into the reservoir, the thermodynamic equilibrium of the reservoir fluids is altered, due to the presence of a new fluid. It results in a process of mass transfer between the phases that were already in the reservoir and the injected phase. This process can be represented by taking values at early times of the experiment. Second, fluids that are already in the reservoir for geological periods are in thermodynamic equilibrium, i.e. the mass transfer between phases is already stabilized. Therefore, a late time measurement must be taken to represent these processes.

As the logarithmic function has no limit when the independent variable approaches infinity, there is a problem in determining its equilibrium value. This can be done assuming that, when the function is at a specific rate of change (i.e. its derivative assumes a threshold value), it is stabilized. However, the subjectivity still exists because one must state a threshold value.

In addition, several factors can affect the dynamic behavior of the IFT between two fluids. The experiments analysed in this work aim to illustrate some of these factors, such as surface-active components and the presence of CO₂.

Given the scenario, this study has aims to analyse the IFT data from DSA technique in a most adequate manner. In addition, to understand the stabilization of IFT under different conditions and to determine if the logarithmic function modeling is possible.

1.2 Structure

This work is subdivided into five chapters

- Chapter 1 discussed the current scenario of enhanced-oil-recovery applications through reservoir engineering.
- In Chapter 2, some of the research previously done is referenced in order to clarify the important concepts to this work.
- The materials and methods are discussed in Chapter 3, covering the samples and procedures used during this research.
- Chapter 4 is about the results acquired from the experiments and data analysis, discussing each of them at three different aspects: the curve fitting to the data, the stabilization time analysis and the comparison between dynamic and equilibrium IFT.
- Chapter 5 contains the conclusions made by this work and purposes for future experiments and work.

CHAPTER 2: LITERATURE REVIEW

2.1 Interfacial Tension

Surface tension (SFT) is a force exerted on the boundary between a liquid and a vapor phase per unit length. This force is due to differences between intermolecular forces from both phases. As the intermolecular interaction is greater when the two molecules belong to the same phase, because they are more similar with respect to polarity, there is a force imbalance at the interface. The greater the dissimilarity between the phases polarity, the greater the tension. This tension is expressed units of force per length (i.e. dyn/cm or N/m). The Interfacial Tension (IFT) is defined analogous to the SFT, but with both phases not being gaseous (SHAW, 2013). Another form to define IFT is the amount of work required to create a new unit of surface area at the interface (CRAFT; HAWKINS, 1990).

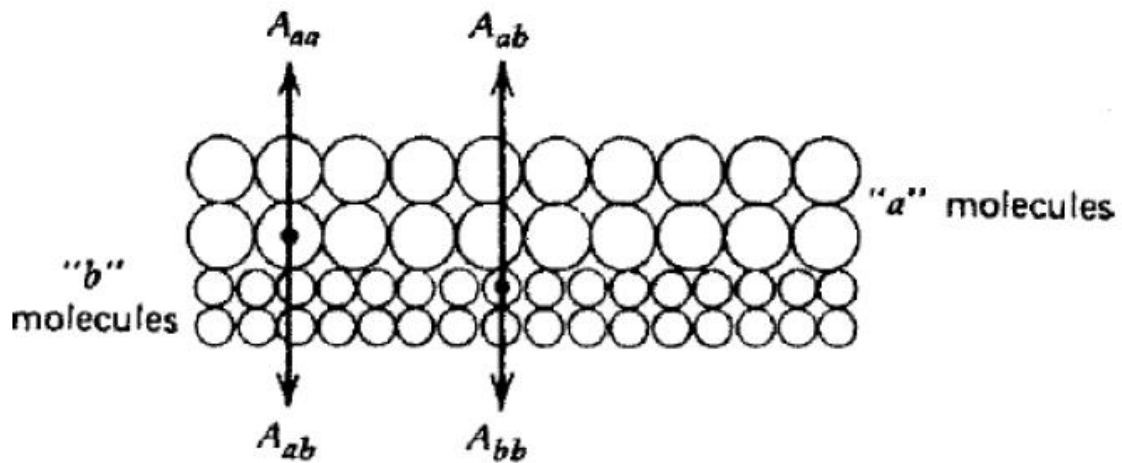


Figure 2 - Scheme of bulk and interfacial interactions between two molecules (ROSEN; KUNJAPPU, 2012)

Rosen and Kunjappu (2012) exemplified this concept with a scheme showed in Figure 2. In this figure, its possible to see that “a” molecules in the bulk interact only with others “a” molecules, while molecules at the surface interact with both “a” and “b” molecules. Then it is possible to define the potential energy of each phase as the difference between their energies interactions.

$$A_{total} = A_a + A_b \tag{1}$$

$$A_a = A_{aa} - A_{ab} \tag{2}$$

$$A_b = A_{bb} - A_{ab} \quad (3)$$

$$A_{total} = A_{aa} + A_{bb} - 2A_{ab} \quad (4)$$

Where A_i represents the potential energy of each phase and A_{ij} represents interaction energy between these components. If one divides both sides of the equation (4) by the interface area " I ", it is possible to define the interfacial tension between both phases.

$$\gamma = \frac{A}{I} \quad (5)$$

$$\gamma_{total} = \gamma_{aa} + \gamma_{bb} - 2\gamma_{ab} \quad (6)$$

Where γ_{total} is the IFT of the system, γ_{aa} and γ_{bb} are the superficial tensions of phases a and b respectively, and γ_{ab} is the interaction energy between both phases by unit area. It is possible to notice that the more similar are the two phases, the greater will be the negative term, consequentially, the smaller will be the interfacial tension between them both. When the IFT between two fluids is near zero, they are considered miscible.

As stated before, IFT is the amount of work necessary to increase the interfacial area by one. Hence, it is possible to define:

$$\gamma = \left(\frac{\partial G}{\partial A} \right)_{T,P,n} \quad (7)$$

Where G is the Gibbs free energy and A the surface area between both fluids. A spontaneous evolution at constant temperature and pressure results in a decrease in Gibbs free energy (DE GENNES; BROCHARD-WYART; QUÉRÉ, 2004). Since the molecules at the interface contain greater potential energy than those at the bulk, the natural way to reduce Gibbs free energy is to minimize the number of molecules at the interface. This is the reason why immiscible fluids tend to segregate after a while as shown in Figure 3.

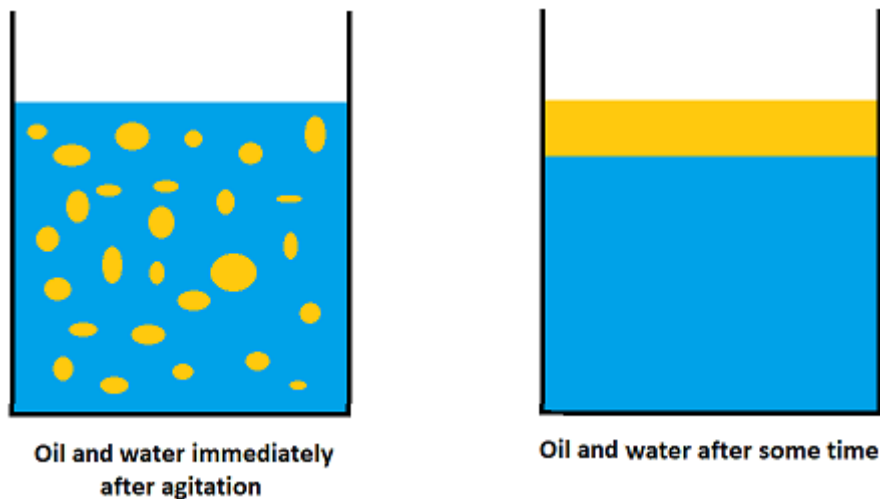


Figure 3 - Scheme of phase segregation

The intermolecular forces that act in the IFT are strongly dependent on the type of fluid and its chemical nature (FOWKES, 1964). The London dispersion forces exist in all types of matter and are responsible for part of the attractive force between adjacent molecules (HAMAKER, 1937). These forces are generated from interactions of fluctuating electronic dipoles with induced dipoles in neighboring molecules. The attractive forces in a saturated liquid hydrocarbon can be entirely represented by the London dispersion forces. For another substances with different chemical nature (e.g. brines and crude oils), other intermolecular forces take place. These can be the dipole-dipole interactions, which occurs when the partially positively charged part of molecule interacts with the partially negatively charged part of the neighboring molecule. And the hydrogen bonding, which is a special kind of dipole-dipole intraction that occurs specifically between a hydrogen atom bonded to either an oxygen, nitrogen, or fluorine atom (FOWKES, 1964).

As mentioned before, the IFT is one of the most important parameters that have impact on the RF. Capillary pressure is responsible for trapping the residual oil after a 100% efficient waterflooding procedure. There is a strong relation between capillary forces and interfacial tension, and this dependence can be estimated by the Young-Laplace equation showed in Equation (8).

$$\Delta P = \gamma \left(\frac{1}{R_1} + \frac{1}{R_2} \right) \quad (8)$$

Where ΔP is the capillary pressure, γ is the interfacial tension between both fluids and R_i are the main radii of curvature.

It is possible to see by Equation (8) that the higher the IFT between fluids, higher the capillary pressure trapping oil at the pores of rock. In addition, the size of the pores has a role as well, since the smaller the pore, the larger will be the capillary pressure. Thus, in an oil-wet heterogeneous rock, the sites with smaller pores will be the ones with more oil retained.

The role of IFT in the recovery of a reservoir comes when one is trying to displace the oil phase from rock pores with an aqueous phase. The Capillary Number evaluates the microscopic recovery efficiency. This number is a dimensionless number created to estimate the effects of capillary forces against viscous forces. As it takes account for capillary forces, it is closely related to the displacement efficiency.

$$N_c = \frac{v\mu_w}{\gamma\cos(\theta)} \quad (9)$$

Where N_c is the Capillary Number, v is the velocity of the displacing fluid, μ_w is the viscosity of the displacing fluid, γ is the IFT between both fluids and θ is the contact angle formed at the interface between both fluids and the rock wall, measured through the fluid of higher density.

Thus, to enhance the oil recovery it is necessary to raise the water viscosity for controlling the mobility ratio – until the additional friction loss generated do not exceed the pump pressure limit at the site – as well as reducing the interfacial tension between both fluids, consequentially increasing the Capillary Number. Figure 4 shows the capillary desaturation curve, that represents the residual oil saturation for a given Capillary Number.

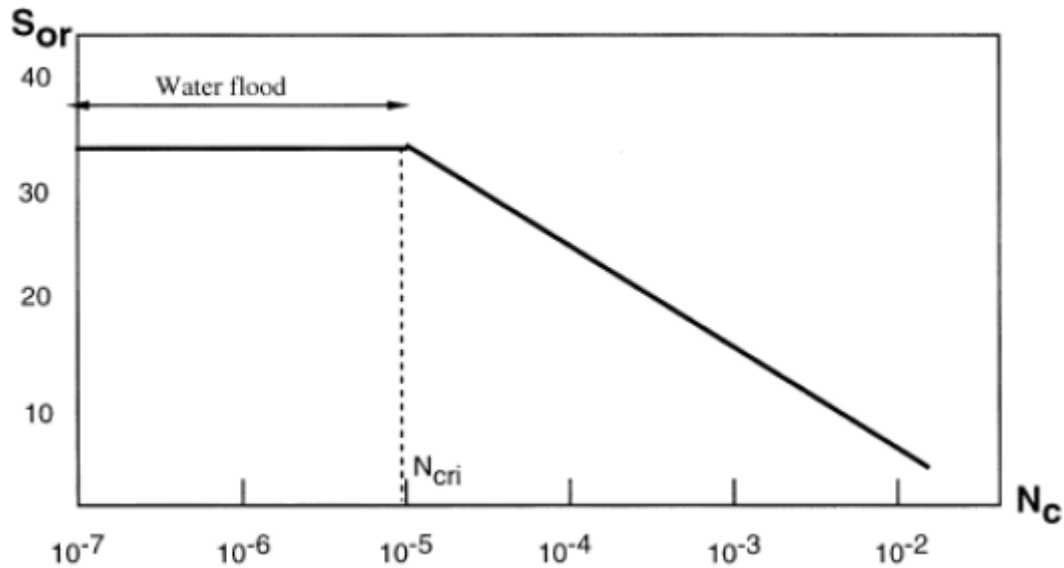


Figure 4 - Capillary desaturation curve for a water-wet rock (SHOSA; SCHRAMM, 2001)

It is visible that there is a threshold value for the Capillary Number called Critical Capillary Number. Below this value, alterations in the IFT will result in no alteration of the residual oil saturation (S_{or}). The shape of this curve depends on several parameters, such as pore size distribution (PSD) and wettability. Since after the waterflooding process, the N_c is normally lower than the critical value, it takes a great reduction in the IFT to reduce the ROS. This reduction is achieved usually by the using of surfactants within the drivin fluid, in chemical EOR methods (SHOSA; SCHRAMM, 2001).

2.1.1 Surface-active agents

Surfactants (abbreviation for surface-active agents) are amphiphilic molecules (i.e. are soluble in two different phases, such as oil and water) and act lowering the interfacial tension of the system. They are composed of a polar (hydrophilic) head, and a non-polar (lipophilic) tail and these features give the amphiphilic ability to those molecules (ROSEN; KUNJAPPU, 2012).

The name surfactant usually refers to the synthetic molecule that is fabricated for many purposes, for example, used in daily products like detergents, shampoos, soaps, etc. or petroleum industry related aspects, like surfactant flooding into a reservoir. However, there are natural surfactants present in nature and they have a role into IFT measurements in some cases.

Crude oils are composed of various compounds including paraffins, aromatics, resins and asphaltenes. A Saturates, Aromatics, Resins and Asphaltenes (SARA) analysis can determine the concentration of each in the oil. A schematic illustration of this classification is shown in Figure 5.

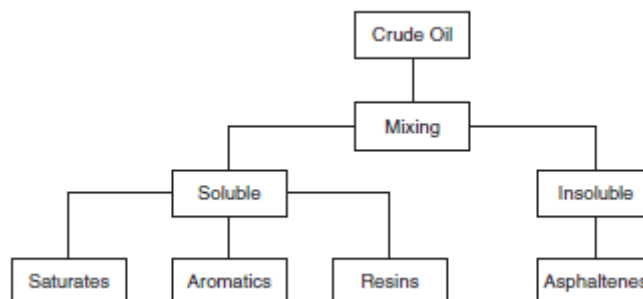


Figure 5 - Scheme of SARA classification of crude oil (GUDMUNDSSON, 2017)

Paraffins and aromatics are non-polar hydrocarbon chains, i.e. there is no significant amount of charge difference along with the molecule length. Resins consist of large relative polar molecules, often containing heteroatoms such as sulphur, nitrogen and oxygen. Asphaltenes are the larger molecules that contain the largest amount of heteroatoms (GUDMUNDSSON, 2017).

Both asphaltenes and resins are similar in structure due to their complexity and presence of heteroatoms, but, as opposite to paraffins and aromatics, they carry a significant electric charge difference along with the molecule length. In addition, the complex structure of the molecules, the presence of heteroatoms together with the charge gradient make these molecules to act like a surfactant. They have polar and non-polar parts (when compared relative to each other) that give both asphaltenes and resins amphiphilicity.

Thus, these components from the oil usually seek for the interface, where their polar part stays in contact with water and their apolar part stays near to oil phase. Due to this, they are responsible for the transition between the phases at the interface. Therefore, they could act reducing the resulting IFT.

2.1.2 CO₂

Carbon dioxide is one of the greenhouse gases emitted by human activity along with CH₄, N₂O and hydrofluorocarbons. It is a fact that even if this compound has a lower warming potential compared to the other gases, CO₂ is the highest in terms of both

emissions and impact. The Brazilian Pre-salt reservoirs have a content of CO₂ up to 20% of the produced gas (CEZAR et al., 2015). The effects of CO₂ dissolution on the pH of the ocean is still uncertain (TAMBURRI et al., 2000), so, one solution is the use as a process fluid in oil and gas reservoirs (YANG; GU, 2005).

CO₂ flooding process will have impact in some characteristics of the reservoir fluid, such as densities, viscosities and interfacial tension. It was found that these processes can enhance oil recovery normally by up to 8-16% of the OOIP (GRIGG; SVEC, 2008). In addition, the cost of carbon dioxide injection is low compared with natural gas or nitrogen (KLUSMAN, 2003).

As CO₂ is injected into the reservoir by a continuous flooding or an alternating method (e.g. water alternating gas or WAG) it partitions (i.e. divides itself) into oil and water phases, respecting their solubilities (GEORGIADIS et al., 2011). This phenomenon generates changes in the fluids properties, such as density and viscosity. Depending on the type of crude oil and brine present at the reservoir, the impact on density will be different (DREXLER et al., 2018).

Sun and Chen (2005) studied the impact of CO₂ on interfacial tension between a live oil and brine. They used a low salinity brine and a heavy live oil from a Chinese reservoir to do their experiments. They measured the IFT as a function of pressure for different carbon dioxide concentrations. The conclusions were that IFT values decreased with increasing CO₂ content and pressure had a minor effect on the measured IFT. However, depending on oil and brine composition and the pH of the aqueous phase, the CO₂ can even increase the IFT of the system (LASHKARBOLOOKI; AYATOLLAHI, 2018).

2.1.3 Density

Densities of fluids are of paramount importance to IFT measurements. Different authors have been used different considerations regarding their fluid densities. In H₂O + CO₂ systems, several authors considered the density of each fluid to be equal to the pure component density (DA ROCHA; HARRISON; JOHNSTON, 1999; HEBACH et al., 2002). On the other hand, some authors used constant density for the water phase only (JHO et al., 1978; MASSOUDI; KING, 1974). Bachu and Brant Bennion, in 2009, used experimentally measured data for both fluids.

The difference between densities of both fluids has a large effect on the IFT measured using the DSA method. Therefore, choosing the most adequate density considered is extremely important to acquire a reliable measurement. Even well known

fluids, such as pure water, will have its density altered after placed in contact with a different fluid, due to mass transfer between both phases. (GEORGIADIS et al., 2010).

2.1.4 Pendant drop method

Many methods have been developed to determine IFT values, but the pendant drop method is most suitable for measuring IFT at high pressures and temperatures conditions. Traditionally, this method determines the IFTs by photographing a pendant drop and then measuring the drop dimensions from negative films. This implies that experimental results were inherently inaccurate, depending on the resolution of the microscope used and the subjectivity of the operator (YANG; GU, 2005). In the literature, the DSA technique was employed to measure the equilibrium IFTs of various systems under reservoir conditions (RAO; LEE, 2003).

The theoretical background for the calculation of the IFT value from the profile of a pendant drop was already discussed in the literature (ANASTASIADIS et al., 1987). So, a briefly outline of the theory will be shown here.

After a period of time, the liquid pendant drop reaches hydrodynamic and mechanical equilibrium with the bulk phase. This equilibrium is governed by both gravitational force and interfacial tension. The resulting profile is shown in Figure 6.

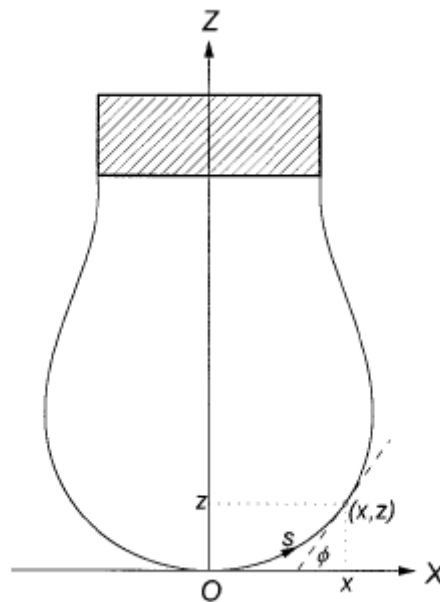


Figure 6 - Pendant drop profile (SONG; SPRINGER, 1996)

This profile can be described by the following equations:

$$\frac{d\phi}{dS} = \frac{2}{B} - Z - \frac{\sin(\phi)}{X} \quad (10)$$

$$\frac{dX}{dS} = \cos(\phi) \quad (11)$$

$$\frac{dZ}{dS} = \sin(\phi) \quad (12)$$

With the boundary conditions at the drop apex

$$X = Z = S = \phi = 0 \quad (13)$$

$$\frac{\sin(\phi)}{X} = \frac{1}{B} \quad (14)$$

Where

$$B = \frac{1}{ak_{apex}} \quad (15)$$

$$a = \sqrt{\frac{\gamma}{\Delta\rho g}} \quad (16)$$

Equations (10), (11) and (12) are a special form of the general Laplace-Young equation (8) of capillarity in the case of a pendant drop. The variables X, Z and S are the dimensionless forms of the corresponding dimensional variables x, z and s indicated in Figure 6. They are related to each other by the following equations:

$$x = X \cdot a \quad (17)$$

$$z = Z \cdot a \quad (18)$$

$$s = S \cdot a \quad (19)$$

Where a is often known in the literature as the capillary constant. It is a constant for a given liquid-liquid or liquid-gas system. B is called the shape parameter of drops,

which alone determines the dimensionless drop profile as can be seen in equations (10), (11) and (12). Both B and a together define the dimensional drop profile. $\Delta\rho$ is the density difference between the drop and the bulk phase, g is the gravitational acceleration and γ is the IFT value one is trying to determine.

Regarding the shape parameter of drops, a value between 0.6 and 0.7 are desirable for better results. Drop profiles with small B values ($B < 0.5$) are almost spherical and have little gravitational effects. While drop profiles with large B values ($B > 0.75$) are relatively short and can easily deattach from the needle (SONG; SPRINGER, 1996).

2.1.5 Dynamic behavior

As soon as two phases are in contact, a mass transfer process begin. This mass transfer tends to equilibrate the chemical potential of different components in both phases. Surface-active species tend to diffuse to the interface between the fluids to minimize the free energy of the whole system (ROSEN; KUNJAPPU, 2012). This diffusion process can take up to days depending on the composition of each phase, so a dynamic behavior takes place.

This time-dependent decay of IFT is due to the migration of the amphiphilic compounds to the interface. Thus, IFT decays drastically during the first moments after the drop formation and its derivative declines within time, until it approaches 0. Thus, the IFT value reaches a plateau called equilibrium IFT. These surface-active components are, in case of an oil and water measurement, mostly asphaltenes, resins and impurities.

Susnar et al., in 1994, investigated the n-decane + water system at high pressures and ambient temperature using the axisymmetric drop shape analysis (ADSA) method. They stated that the density dependence resulting from diffusion of one phase into the other is negligible, therefore, it was assumed that the densities of both fluids were those of the pure components. They concluded that is impossible to be sure that no impurities exist in the system, and the values taken immediately after the drop's formation are the more reliable ones. However, this will only be true if both fluids have been previously saturated with each other. Thus, this assumption could never be done in a crude oil x brine system (GEORGIADIS et al., 2011).

2.2 Data analysis

2.2.1 Curve fitting

Curve fitting is defined as the process of constructing a curve, or mathematical function, which has the best fit to a series of data points (HALLI; RAO, 2013). This can involve either interpolation, a method of constructing new data points within the range of a discrete set of known data points; and smoothing, defined as the creation of an approximating function that attempts to capture important patterns in the data set, while leaving out noise.

Fitting functions to data points are usually made on the form:

$$y = f(x) \quad (20)$$

Where y is what one is measuring, the dependent variable, and x is the independent variable, usually position or time.

Several functions are used to fit data sets, including polynomial, exponential, logarithmic, trigonometric, etc. The best fitting function will depend on the curve one is trying to fit, i.e. the distribution of one's data set through the domain will dictate the curve shape, and therefore, the function that fits it with the least error.

Logarithmic functions are defined as:

$$y = a \cdot \ln(x) + b \quad (21)$$

Where a and b are the function coefficients which will govern its shape and value.

In this work, the logarithmic function will be used to model the IFT measurements with time lapse. Then, it is possible to define:

$$\gamma = a \cdot \ln(t) + b \quad (22)$$

Where γ is the Interfacial tension, t is the time, and a and b are the fitting parameters.

Extrapolation is a process used to estimate values that are beyond the measured range. It is similar to interpolation, which estimates values between known data, but with more uncertainty. There is an interest in extrapolating the data points so it would be possible to calculate the IFT value for large times (ARMSTRONG; COLLOPY, 1993).

Besides the experimental errors, both curve fitting and extrapolating are processes that generate uncertainty into data analysis. These uncertainties can cause wrong interpretations and conclusions for a given data set. Thus, one must be careful when propagating those uncertainties to the further steps of analysis.

2.2.2 Gaussian distribution

In statistics, the Gaussian (or normal) distribution is a continuous probability distribution. This distribution is useful because of the central limit theorem. This theorem states that, under some conditions (finite variance, unbiased sampling, etc.), the averages of the samples of observations of random variables independently drawn from independent distributions converge to the normal (i.e. they become normally distributed when the number of observations is sufficiently large) (LYON, 2013).

The empirical rule is used to represent the percentage of values that lie within a band around the mean in a normal distribution. It states that 68.27% of the values lie within one standard deviation of the mean; 95.45% at two standard deviations; and 99.73% at three standard deviations. These values are derived from probability calculations using the Gaussian distribution (O'CONNOR, 1990). This concept is illustrated in Figure 7.

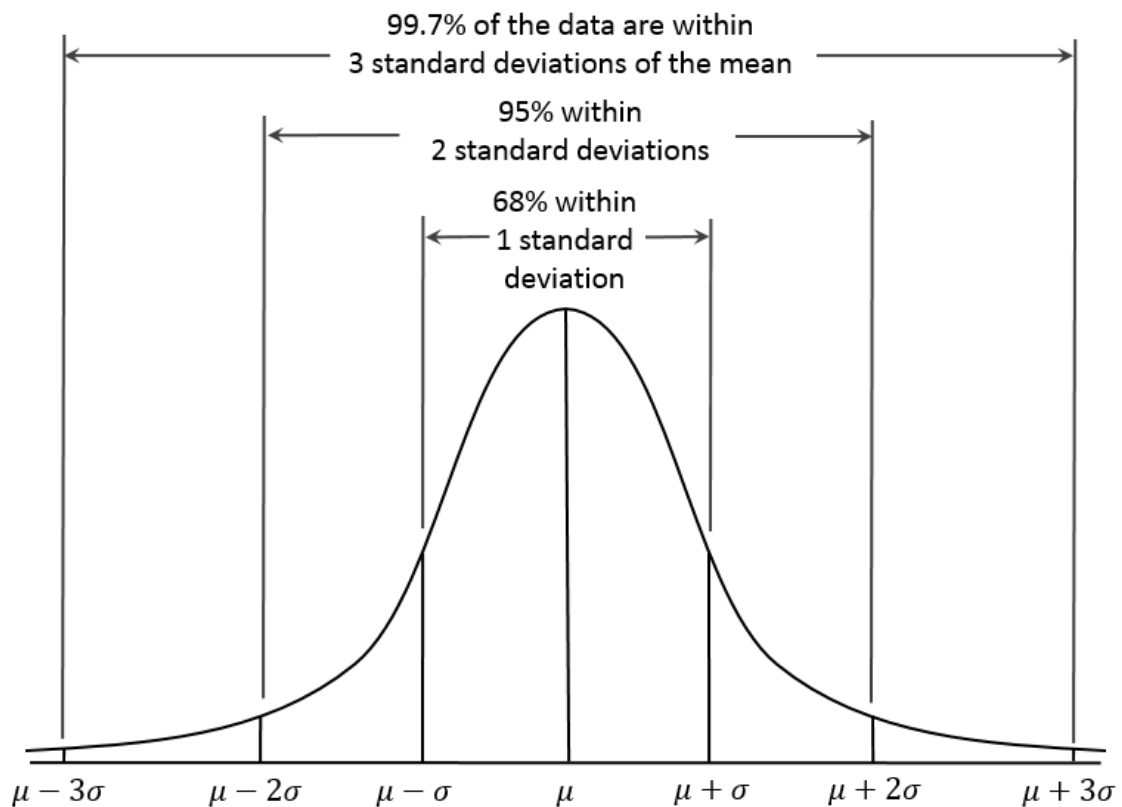


Figure 7 - Empirical rule for normal distributions

These are relevant concepts for this work because they will be used to analyse the data acquired and help to exclude the outliers from the results.

2.2.3 Coefficient of determination

The R^2 value has an important role in this work, because they are useful to identify the fitting performance. A perfect fitting of the curve to the data points has R^2 equal to 1. In contrast, a coefficient of determination close to 0 means that the function does not fit the data set well.

The values of R^2 are calculated by the least-squares regression. The best fit in the least-squares sense minimizes the sum of squared residuals. The square residuals are the difference between an observed value and the fitted value provided by the fitting function.

CHAPTER 3: MATERIALS AND METHODS

3.1 Materials

The materials used during the tests were:

- **Deionized water (DW)** - The water utilized was purified in laboratory with the water purifier system of reverse osmoses from Gehaka® - model OS10LXE. It's purity after the treating was 0,05 µS/cm at 25°C.
- **Salts** - The salts utilized were acquired from *Sigma-Aldrich* and have more than 99% of purity. The products used in the preparation of the synthetic brine were: NaCl, CaCl₂.2H₂O, MgCl₂.6H₂O, KCl, BaCl₂.2H₂O, SrCl₂.6H₂O e Na₂SO₄.
- **Solvents** - The solvents utilized were n-hexadecane and toluene, acquired from *Sigma-Aldrich*, with purity of 99.9%.
- **Crude Oil (Field B)** - Oil B is a Pre-salt dead crude oil provided by Shell Brasil Ltda. Its characterization is shown in Table 1.
- **CO₂** - The CO₂ utilized has purity of 99.999% and was provided by Praxair.

3.2 Materials characterization

This work is composed of several fluid samples that will be explicit in the following topics. To sum up, there is only one brine phase (Brine B), so it is possible to compare the measurements with each other. In addition, two types of model oil were used (Model oil I and II), and one dead crude oil from Brazilian Pre-salt. Finally, CO₂ was also used during this work.

3.2.1 Brine B

As mentioned before, the synthetic formation water is composed of a variety of sodium and chloride salts. The ionic composition is shown below.

Table 1 - Ionic composition of brine B (DREXLER et al., 2019)

| Ions | Concentration [ppm] |
|-------------------------------|---------------------|
| Na ⁺ | 57,580 |
| Ca ²⁺ | 24,250 |
| Mg ²⁺ | 2,120 |
| K ⁺ | 1,200 |
| Ba ²⁺ | 24 |
| Sr ²⁺ | 1,260 |
| SO ₄ ²⁻ | 54 |
| Cl ⁻ | 139,900 |
| TDS | 226,388 |

The density of brine B at 60 °C with varying pressure was acquired by simulation using OLI Studio[®]. Table 2 shows densities for both brine B and brine B recombined with CO₂.

Table 2 - Brine B density

| Pressure [psi] | Density [g/cm ³] | |
|----------------|------------------------------|------------------------------|
| | Brine B | Brine B with CO ₂ |
| 1000 | 1.182 | 1.183 |
| 2000 | 1.184 | 1.185 |
| 3000 | 1.186 | 1.188 |
| 4000 | 1.189 | 1.192 |
| 5000 | 1.193 | 1.197 |

3.2.2 Model Oil I

Model oil I is an oil essentially paraffinic. It is composed only by n-hexadecane and was not mixed with carbon dioxide during the tests. The density of Model oil I at various pressures and 60 °C was acquired by simulation using PVTsim from Calsep. Table 3 shows the density for Model Oil I.

Table 3 - Model Oil I density

| Pressure [psi] | Model Oil I |
|----------------|------------------------------|
| | Density [g/cm ³] |
| 1000 | 0.761 |
| 2000 | 0.768 |
| 3000 | 0.778 |
| 4000 | 0.779 |
| 5000 | 0.783 |

3.2.3 Model Oil II

Model oil II is the mixture of n-hexadecane (71.1 wt%) and toluene (28.9 wt%). It represents an oil with both paraffinic and aromatic compounds ideally. This oil was mixed with CO₂ so it is possible to compare the results from the tests with and without CO₂ in the system. The density of both dead and model oil II recombined with CO₂ are shown in Table 4 for several pressures and 60 °C. Simulations with PVTsim[®], from Calsep, determined these densities.

Table 4 - Model Oil II densities

| Pressure [psi] | Density [g/cm ³] | |
|----------------|------------------------------|-----------------------------------|
| | Model Oil II | Model Oil II with CO ₂ |
| 1000 | 0.773 | 0.756 |
| 2000 | 0.782 | 0.778 |
| 3000 | 0.789 | 0.796 |
| 4000 | 0.795 | 0.810 |
| 5000 | 0.801 | 0.823 |

3.2.4 Oil B

Oil B is a dead crude oil (API° 26.14) from the Brazilian Pre-salt field B, which has its Saturates, Aromatics, Resins and Asphaltenes (SARA) analysis shown in Table 5 (DREXLER et al., 2019).

Table 5 - Oil B SARA analysis

| Oil B | wt% |
|-------------|-------|
| Saturates | 64.06 |
| Aromatics | 25.98 |
| Resins | 8.46 |
| Asphaltenes | 1.50 |

The density of oil B at several pressures and 60 °C is shown in Table 6. Simulations with PVTsim[®], from Calsep, calculated the densities shown below.

Table 6 - Oil B density

| Pressure [psi] | Oil B |
|----------------|------------------------------|
| | Density [g/cm ³] |
| 1000 | 0.878 |
| 2000 | 0.881 |
| 3000 | 0.883 |
| 4000 | 0.885 |
| 5000 | 0.887 |

3.3 Samples preparation

The experimental procedure used in this study can be divided into two steps: the preparation of fluid samples and the IFT measurements by the pendant drop method on the Drop Shape Analyser (Model DSA 100HP acquired from Kruss).

3.3.1 Formation Water

The brine utilized in this work was prepared in laboratory following the original formation brine composition from field B, as shown in Table 1. A spreadsheet on Excel[®] elaborated by the laboratory team was used on the preparation process as a way of calculating the mass of each salt necessary to emulate the original formation water ionic composition.

After the theoretical masses of each salt have been calculated, it is necessary to weight them on analytical balances from Mettler Toledo[™] New Classic MS. Glass bechers are used to mix the already dissolved salts. After all salts have been dissolved, DW is added to adjust the salinity. Finally, the sample is taken to a magnetic stirrer from IKA[®]C-MAG HS 7 to guarantee homogeneity and total dissolution.

Due to uncertainties involved in this process, all measured values are re-inserted in the calculation spreadsheet so it is possible to estimate the real ionic composition of the prepared brine. Besides that, a conductivitymeter SevenExcellence[™] from Mettler Toledo was used to characterize the sample's conductivity.

3.3.2 Model oil II

The model oil II was prepared mixing n-hexadecane (71.1 wt%) and toluene (28.9 wt%).

3.3.3 CO₂ dissolution in fluids

The combination of fluids with carbon dioxide was necessary for some experiments. The samples are previously degassed for 30 minutes in a vacuum pump nXDS IFT 20 from Edwards. After the sample degassing, carbon dioxide was injected into the piston cell (Proserv) with a booster pump, at a controlled pressure of 1000 psi. Then, the piston cell was agitated to homogenize the fluids within and set to rest for at least one day before the test.

3.4 Density determination

The software PVTsim[®] Nova 3.3, from Calsep, was used to estimate the density of all oily mixtures. Soave Redlich-Kwong (1972) with Peneloux volume correction (1982) was the equation of state (EOS) used to simulate the fluids' densities. In addition, the lumping scheme used was "CO₂ EOR model".

OLI Studio[®] 9.6, from OLI Systems, inc, was used to simulate the density of the brine phase. The aqueous package was used to estimate the density of the dead brine. Furthermore, the Mixed Solvent Electrolytes + Soave-Redlich-Kwong (MSE-SRK) was used to calculate the density of the mixture brine b + CO₂.

3.5 Pendant drop experiment

The experiment was carried out with the HPHT DSA apparatus. The two fluids are stocked in piston cells and connected to the equipment by high-pressure lines. The equipment is composed of several lines and valves, used to control the fluid flow in it; a high-pressure chamber that is sealed with two transparent windows to allow light to pass through and has a temperature controller; a camera and a light source in opposite sides for the imaging capture. In addition, there are two pairs of Quizix pumps (Chandler Engineering) to pump the fluids and control the pressure. The apparatus scheme is shown in Figure 8. For this work, fluids with and without CO₂ were used. The detailed procedure can be found elsewhere (DREXLER et al., 2019).

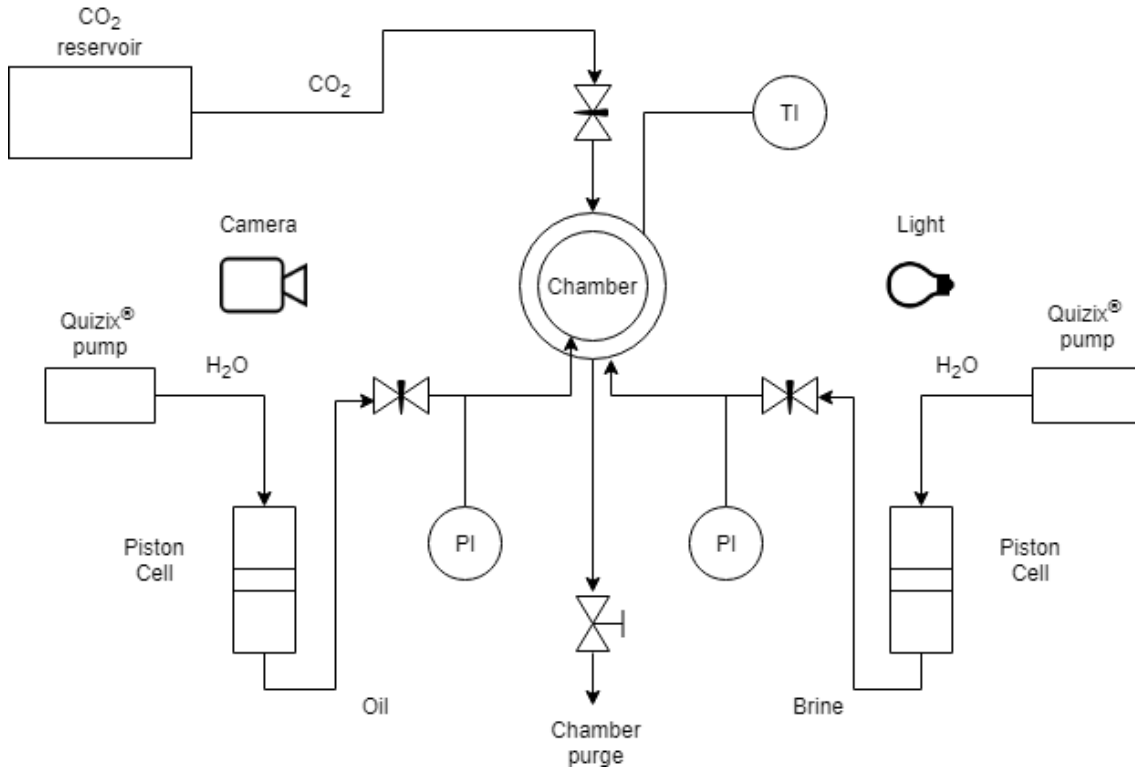


Figure 8 - DSA apparatus scheme

A software from Kruss is used to capture the drop image and calculate the IFT values at each 30 seconds. It analyses the shape of the drop and tries to fit a curve around it. Every value is recorded and can be exported to a comma separated value (.csv) file.

Before the tests, both fluids density must be input into the software. However, as density changes with pressure it would be necessary to input both densities every time the pressure changed. To simplify this process, the density of the bulk phase is considered to be 1, because it represents the heavier phase in this case, and the density of the drop phase is considered to be 0. Due to this approximation, the values read by the software have no physical meaning and must be corrected afterwards. This correction is done simply using the equation (23):

$$IFT_{real} = IFT_{measured} \cdot \frac{\Delta\rho_{real}}{\Delta\rho_{set}} \quad (23)$$

Where $\Delta\rho_{real}$ is the difference between the the real value of both fluids' densities and $\Delta\rho_{set}$ is, as stated before, the difference set in the software which is equal to 1.

3.6 Data analysis

After the test is completed, the results must be treated before interpretation. A macro was made in Visual Basic for Applications (VBA) on Excel®, to handle all data systematically. To exemplify the method, an experiment almost 70 hours long will be used. This experiment was taken at 60°C and 3000 psi, and the fluids were dead oil B and brine B.

First, the raw data was smoothed by an average of each 50 measurements in a way to minimize outliers and oscillations that could hinder the curve shape. This averaging range was chosen so it is possible to standardize data management. It is possible to notice in Figure 9 and Figure 10 that the data dispersion is smoothed, but the trend of the curve stays the same.

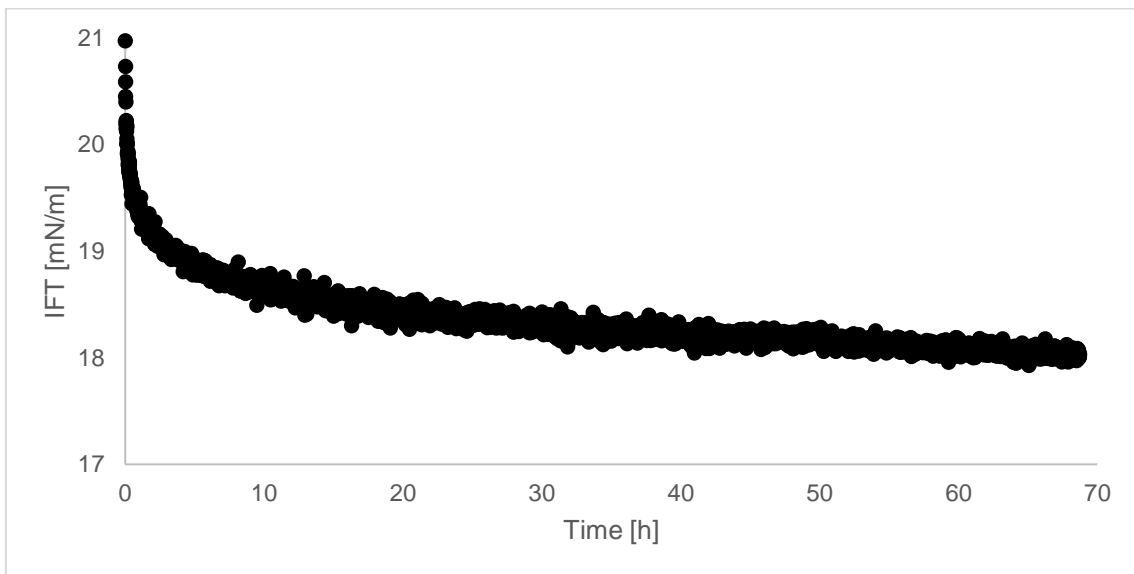


Figure 9 - Oil B + Brine B untreated scattered data

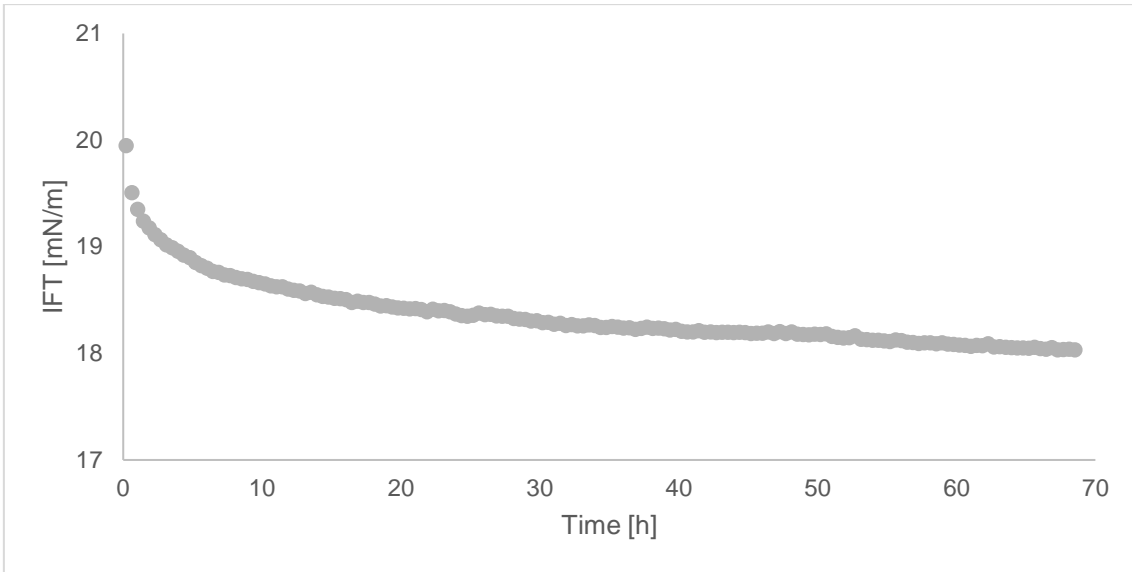


Figure 10 - Oil B + Brine B smoothed scattered data

After smoothing the data set, a logarithmic function was used to represent the data continuously. This allows to obtain the equation that best represents the discrete data from the experiment, along with the R^2 . Figure 11 shows the equation and R^2 for the example.

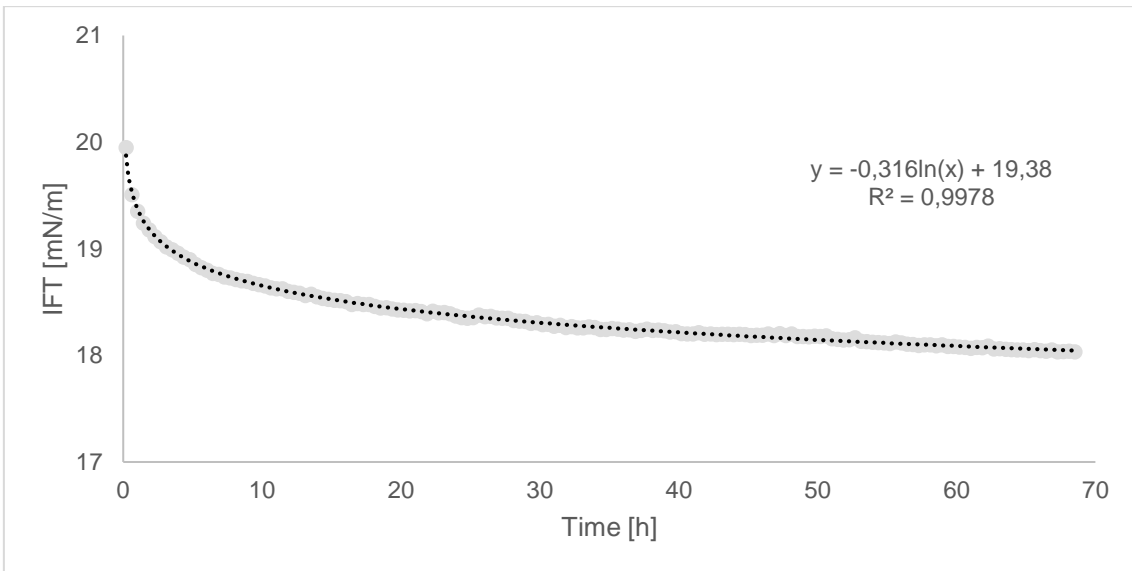


Figure 11 - Oil B + Brine B fitting function with equation and R^2

It might be possible to use this equation instead of real data points to get some critical values. To test the accuracy of this approximation, the same procedure was carried out using the data from the first 5 hours only. Figure 12 shows the cropped curve and the new equation that best fits the new set of data.

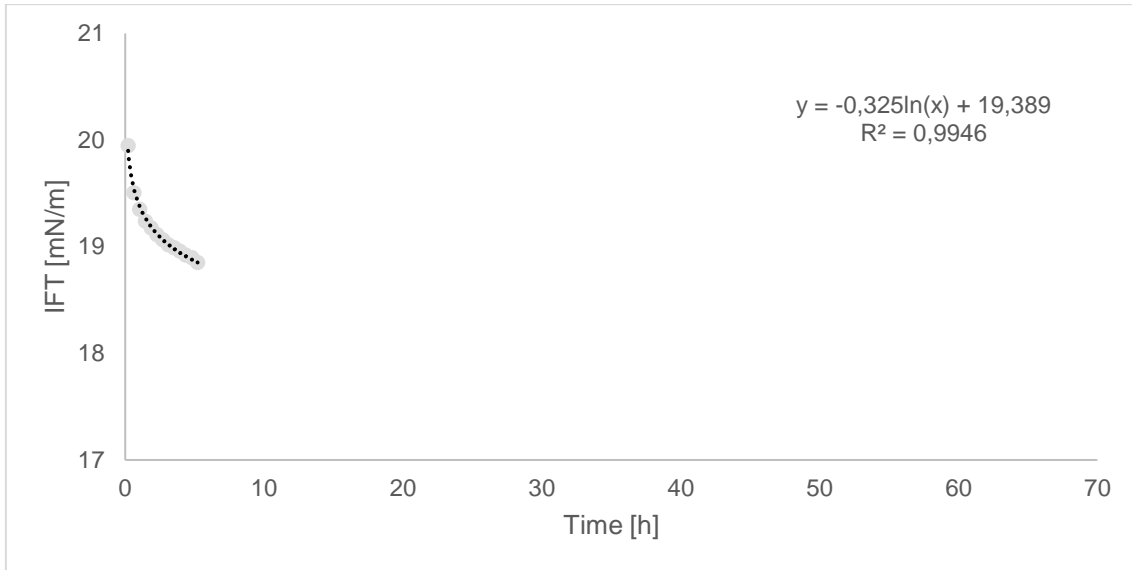


Figure 12 - Oil B + Brine B first five hours of measurement

Comparing both Figure 11 and Figure 12, one can notice a difference in their fitting coefficients. This is owing to the different data set present in each case. It is logical that comparing both functions, the one that had more data to adjust will be the one more reliable. An important question is the relative difference between both functions. Also, how well this functions can model the real data set. Table 7 shows a comparison between the measured IFT and the estimated IFT for both functions, along with their relative errors.

Table 7 - Comparison between measured and calculated IFT

| Time = 60 h | IFT [mN/m] | Relative Error |
|----------------------------|------------|----------------|
| Measured | 18.08 | - |
| Calculated (70 h function) | 18.08 | 0.034% |
| Calculated (5 h function) | 18.05 | 0.120% |

Analysing the table, it is possible to observe that the error made by the first fitting function (70 h function) was almost null. As expected, the relative error of the 5 h function was the highest one. For this example, it is not a high value, though. Therefore, it is possible to estimate accurately the IFT value for a long test, even with only few hours of measured data. This allows more tests to be run for shorter duration.

3.6.1 Stabilization time

The problem of using a logarithmic function to model an experiment is that its limit does not exist when the argument goes to infinity, as shown in Figure 13. Thereby, it is important to define at which point the function does not significantly change its value.

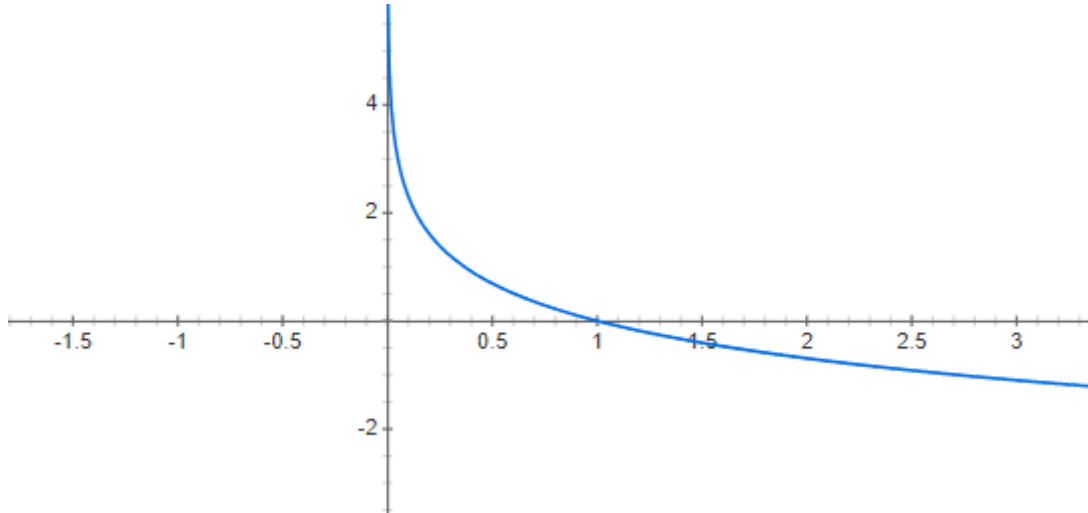


Figure 13 - Plot of a negative logarithmic function

In order to analyse how the value of any function changes at a specific time, it is useful to use its derivative. Thus, the derivative of the logarithmic function is defined as:

$$\gamma = a \cdot \ln(t) + b \rightarrow \frac{d\gamma}{dt} = \frac{a}{t} \quad (24)$$

Using the derivative of the function, a threshold value can be used to calculate the stabilization time. Therefore, if the same threshold value is used, the resulting data will be comparable. In addition, this time value solves the problem of the unlimited function. For this work, the threshold value for the derivative was a subject of study at the results section. As a mean of comparison, the dynamic IFT was calculated as the average between the 150 and 900 seconds measurements (GEORGIADIS et al., 2011).

Considering a normal distribution for the uncertainties of the measurements, they will be calculated as the Standard Error (SE). The SE is calculated by dividing the standard deviation by the square root of the number of measurements.

CHAPTER 4: RESULTS AND DISCUSSIONS

This section is subdivided considering the different type of analyses performed in this work (i.e. curve fitting, stabilization time and comparison between dynamic and equilibrium IFT) comparing the tests with each other. All experiments (but the ones with Model oil II) were repeated at least three times, and their average was considered as the result. The environmental conditions for the tests were a constant temperature of 60° C and pressures from 1000 to 5000 psi. Also, in all tests the aqueous phase is brine B, so the only variable is the oily phase.

4.1 Curve fitting

The objective of this section is to show how well the logarithmic curve fits all systems listed. Visual and mathematical processes through the section will achieve this.

4.1.1 Method validation

The method was applied to the hexane + pure water system, at atmospheric pressure and two temperatures, in order to compare with data from literature. Figure 14 shows the plot of IFT for this system in function of time.

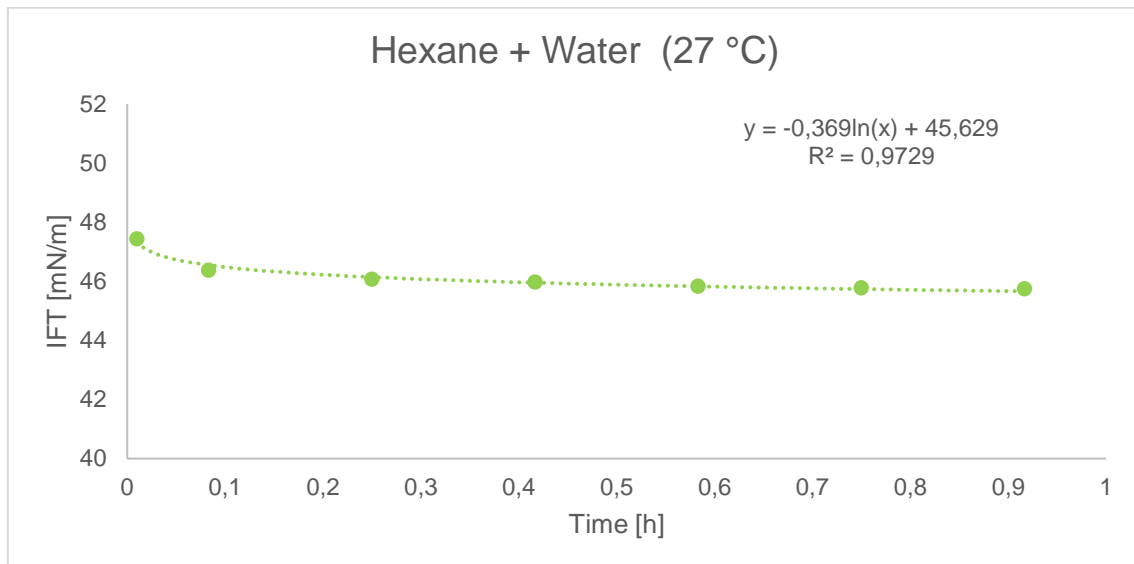


Figure 14 – Experimental IFT of Hexane and water at atmospheric pressure and 27 °C

The R^2 value of the previous logarithmic fitting curve was 0.9729. This is a high value for the coefficient of determination, indicating a good fitting of the data.

Figure 15 shows the relationship of IFT and time for the hexane and water at 14.7 psi and 50 °C. The R² is higher than the previous one, with a value of 0.9924. This means that this test is suitable for this fitting method. However, the comparison between the calculated data must be done in order to validate the output from the fitting function.

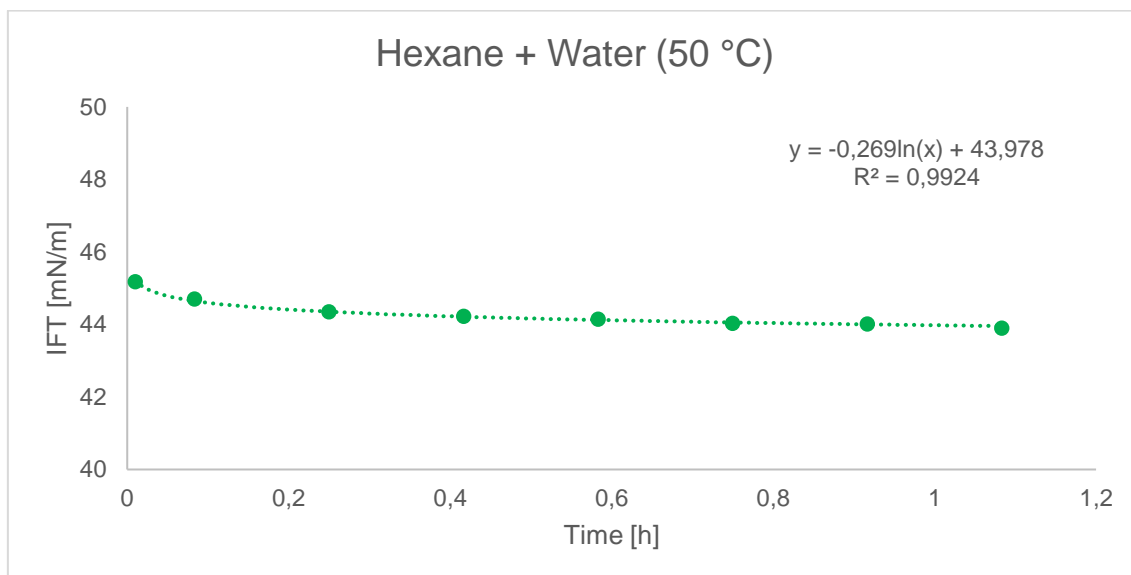


Figure 15 – Experimental IFT of Hexane + water at atmospheric pressure and 50 °C

Table 8 shows the relative error of the calculated data compared with data from Wiegand and Franck (1994). It is possible to notice that the measurement made with lower temperature has a higher error value. The comparison at 50 °C has a good relative error of 3.26%. In fact, both calculated values have a lower value than the reference from literature. This may be due to the presence of impurities from the apparatus in the phases. These impurities act diminishing the equilibrium IFT, because they migrate to the interface. To sum up, the data calculated from the fitting curve gave satisfactory results. Also, the fact that the higher temperature measurement had the lowest error may be due to the high mobility of the molecules.

Table 8 - Comparison between literature and caculated data

| Temperature [°C] | Reference [mN/m] | Calculated [mN/m] | Relative error |
|------------------|------------------|-------------------|----------------|
| 27 | 49.96 | 46.47 | 6.99% |
| 50 | 44.54 | 43.09 | 3.26% |

4.1.2 Fluids without CO₂

4.1.2.1 Model oil I

For the Model oil I, Figure 16 shows a good fitting for the experimental results. The R² equals 0.9691, due to oscillations of the measured points.

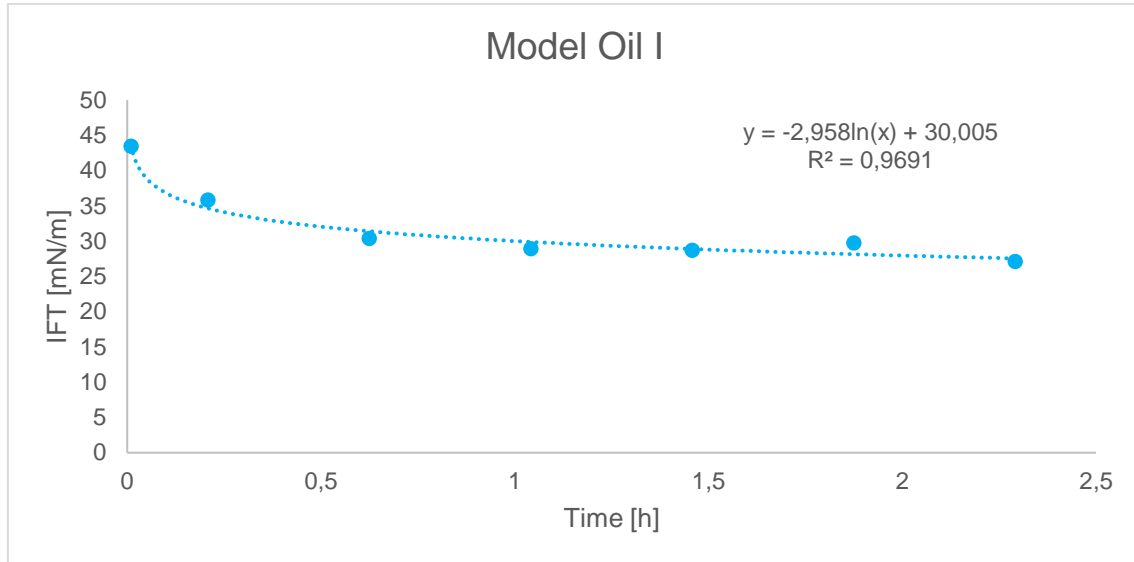


Figure 16 – Experimental IFT of Model oil I x Brine B at 1000 psi

Table 9 shows the different equations and R² coefficients for model oil I x brine B system using a logarithmic fitting.

Table 9 - Equation coefficients for model oil I at 1000 psi

| 1000 psi | 1st | 2nd | 3rd | 4th | Average | Std Dev |
|----------------|--------|--------|--------|--------|---------|---------|
| a | -2.96 | -3.70 | -1.14 | -2.18 | -2.49 | 1.09 |
| b | 30.01 | 27.87 | 39.78 | 37.94 | 33.90 | 5.85 |
| R ² | 0.9691 | 0.9989 | 0.9793 | 0.9385 | 0.9715 | 0.0252 |

Using the four tests made at the same conditions it is possible to show how good the fitting function is modeling the results of the experiment. As stated before and illustrated in Figure 7, assuming a normal distribution and using a range of twice the standard deviation, possible outliers can be identified and removed in order to get a more reliable data. This range contemplates about 95% of all data in a normal distribution. Thus, none of the measurements in Table 9 is considered an outlier. Table 10 shows the range for “a” and “b” coefficients, where “a” and “b” are the coefficients of equation (22).

Table 10 - Range of reliable values for coefficients of model oil I at 1000 psi

| 1000 psi | Min limit | Max limit |
|----------|-----------|-----------|
| a | -4.68 | -0.31 |
| b | 22.21 | 45.59 |

For measurements at 5000 psi, the curve of IFT as a function of time is shown in Figure 17:

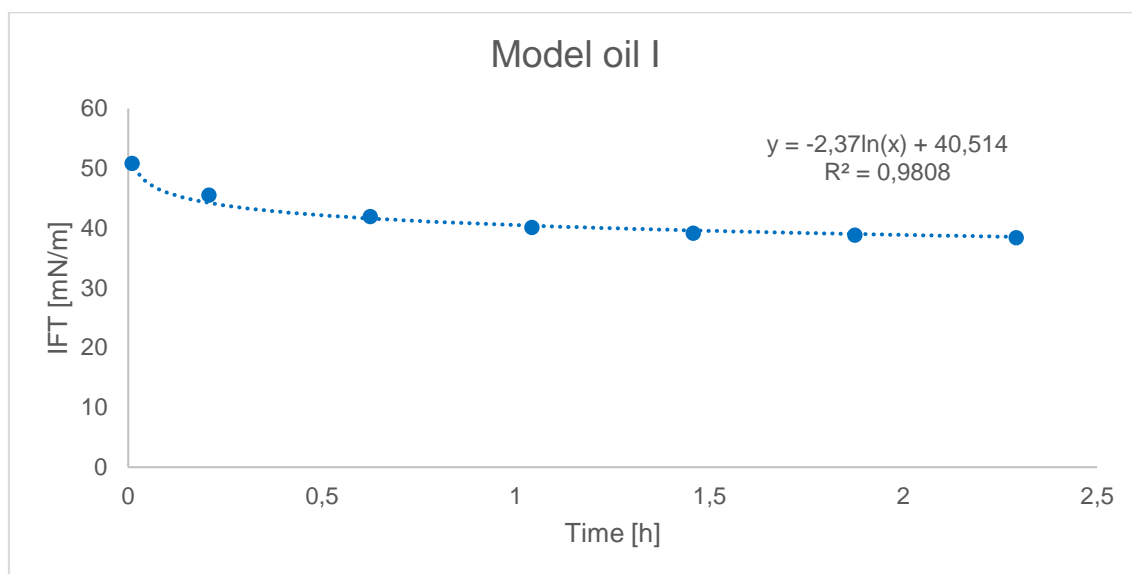


Figure 17 - Experimental IFT of Model oil I x Brine B at 5000 psi

This curve shows a better fitting as the fitting curve passes through more points and R^2 as a greater value. Table 11 shows the coefficients for measurements at 5000 psi.

Table 11 - Equation coefficients for model oil I at 5000 psi

| 5000 psi | 1st | 2nd | 3rd | 4th | 5th | 6th |
|----------|--------|--------|--------|--------|--------|--------|
| a | -2.43 | -1.72 | -2.43 | -2.37 | -2.71 | -0.80 |
| b | 35.75 | 38.47 | 38.01 | 40.51 | 38.18 | 39.87 |
| R^2 | 0.9799 | 0.9065 | 0.9489 | 0.9808 | 0.9941 | 0.6092 |

Among the six experiments shown in Table 11, the 6th results in a R^2 value of 0.6092. This small value of R^2 shows that the model does not represent this experiment properly. Although this measurement lies within the reliable range of twice standard deviation (Table 12), the low value of R^2 excludes the reliability of the fitting curve for this experiment. So, the 6th experiment will not be considered in this analysis.

Table 12 - Average values and reliable limit considering 6th measurement for model oil I 5000 psi

| 5000 psi | Average | Std Dev | Min limit | Max limit |
|----------------|---------|---------|-----------|-----------|
| a | -2.08 | 0.71 | -3.49 | -0.66 |
| b | 38.47 | 1.66 | 35.14 | 41.79 |
| R ² | 0.9032 | 0.1474 | - | - |

Erro! Autoreferência de indicador não válida. shows the average value for the coefficients for 5000 psi without considering the 6th measurement. It is possible to notice the improvement in R² value from 0.9032 to 0.9620.

Table 13 - Average values and reliable limit without considering 6th measurement for model oil I at 5000 psi

| 5000 psi | Average' | Std Dev' | Min limit' | Max limit' |
|----------------|----------|----------|------------|------------|
| a | -2.33 | 0.37 | -3.07 | -1.59 |
| b | 38.18 | 1.69 | 34.80 | 41.57 |
| R ² | 0.9620 | 0.0352 | - | - |

Therefore, with a R² value greater than 0.96 for both experiments (at 1000 and 5000 psi), this system with model oil I (100 wt% n-hexadecane) x brine B is considered suitable for modeling with the logarithmic fitting curve.

4.1.2.2 Model Oil II

Model Oil II is composed of n-hexadecane (71.1 wt%) and toluene (28.9 wt%). Figure 18 shows the behavior of IFT x time with 1000 psi of pressure.

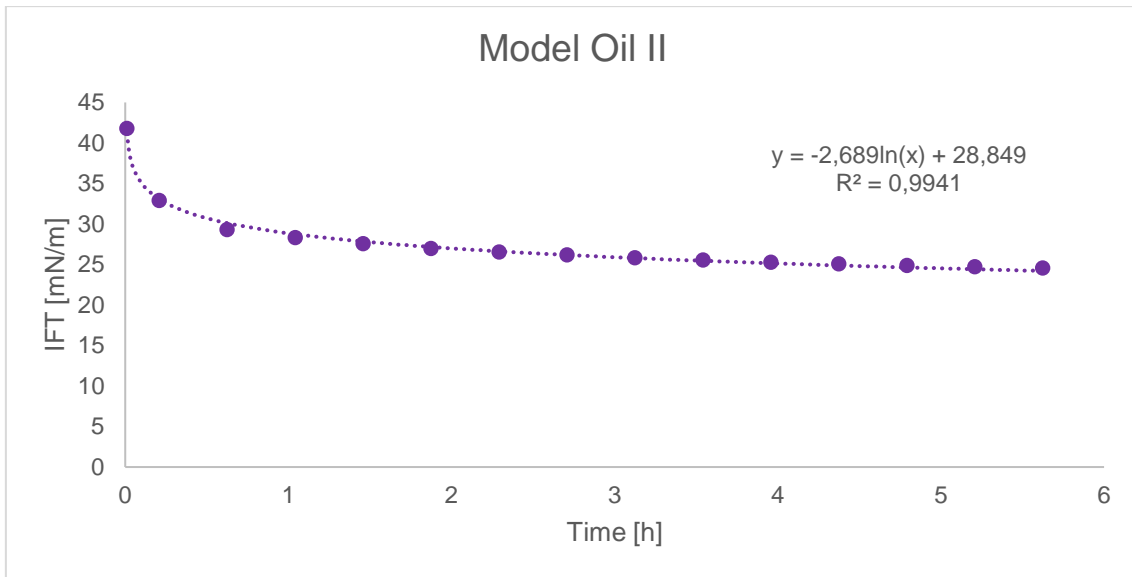


Figure 18 - Experimental IFT of Model oil II x Brine B at 1000 psi

The R^2 value for this example was 0.9941, and the test had almost six hours of duration. It is an almost perfect fitting profile due to the R^2 proximity to 1 (perfect fitting value). Due to time constraints the experiments were not reproduced to increment the consistency of the fitting. This could be carried out in future studies.

Figure 19 shows the behavior of the interfacial tension with time for model oil II at 5000 psi. The R^2 value for this test was also close to 1 ($R^2 = 0.9924$). In fact, both of them show a great potential regarding the logarithmic approximation, due to the proximity of R^2 to 1.

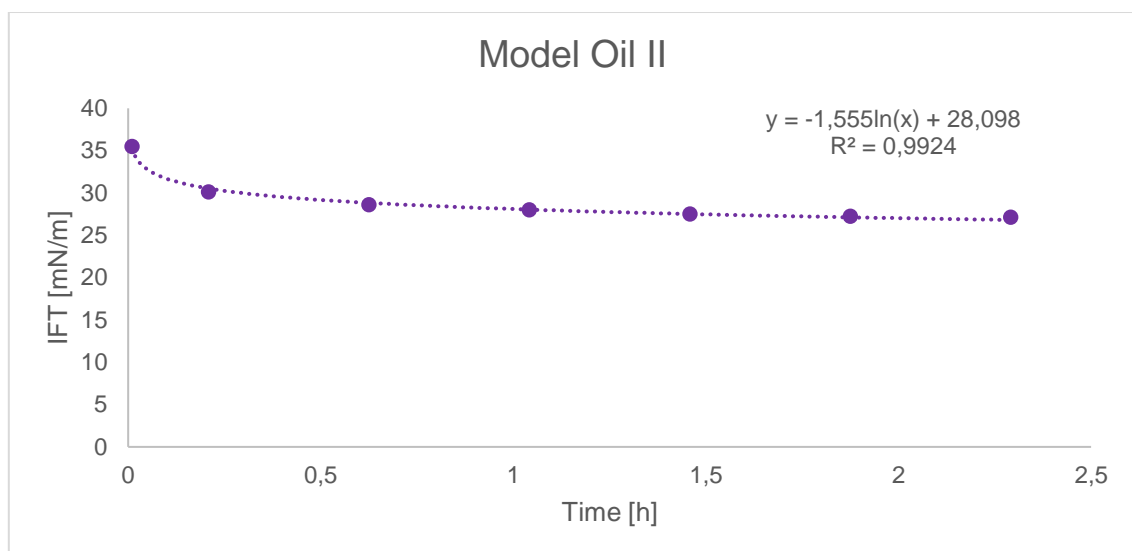


Figure 19 - Experimental IFT of Model oil II x Brine B at 5000 psi

4.1.2.3 Oil B

Figure 20 is showing the time dependence of IFT for Oil B and Brine B system. Once again, the R^2 for this experiment was close to 1 ($R^2 = 0.9951$). This is an indication that this method is suitable for application in crude oils. Oil B contains asphaltenes and resins (surface-active components that have a critical role in IFT measurements) and the presence of both is not affecting the shape of the time decay.

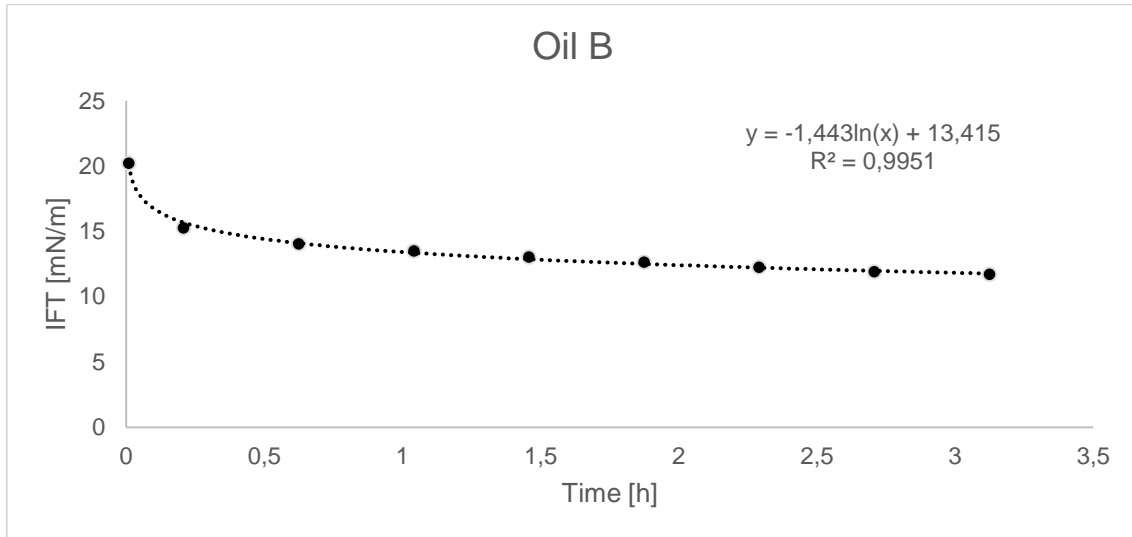


Figure 20 - Experimental IFT of Oil B x Brine B at 1000 psi

Table 14 shows the equation coefficients for oil B x brine B at 1000 psi. The average value of the R^2 equals 0.9834, which means that all tests were fit with good accuracy. This shows the reliability of this method for the system (Oil B x Brine B). It is also noticed that all experiments lie within the reliable range of plus or minus twice the standard deviation.

Table 14 - Equation coefficients for oil B at 1000 psi

| Pressure | Coef. | 1st | 2nd | 3rd | 4th | Average | Std Dev |
|----------|-------|--------|--------|--------|--------|---------|---------|
| 1000 psi | a | -1.44 | -0.19 | -0.97 | -1.09 | -0.92 | 0.53 |
| | b | 13.42 | 14.07 | 15.58 | 15.78 | 14.71 | 1.15 |
| | R^2 | 0.9951 | 0.9647 | 0.9743 | 0.9999 | 0.9834 | 0.0167 |

For this system, several experiments were made at various pressures (1000, 2000, 3000, 4000 and 5000 psi). Table 15 shows the results for all these experiments.

Table 15 - Oil B coefficients for all pressures

| Pressure | Coef. | 1st | 2nd | 3rd | 4th | Average | Std Dev |
|----------|----------------|--------|--------|--------|--------|---------|---------|
| 1000 psi | a | -1.44 | -0.19 | -0.97 | -1.09 | -0.92 | 0.53 |
| | b | 13.42 | 14.07 | 15.58 | 15.78 | 14.71 | 1.15 |
| | R ² | 0.9951 | 0.9647 | 0.9743 | 0.9999 | 0.9834 | 0.0167 |
| 2000 psi | a | -0.25 | -1.22 | -0.84 | -1.44 | -0.94 | 0.52 |
| | b | 14.11 | 15.73 | 14.71 | 13.56 | 14.53 | 0.93 |
| | R ² | 0.9929 | 0.9927 | 0.9178 | 0.9165 | 0.9550 | 0.0437 |
| 3000 psi | a | -0.32 | -0.94 | -1.21 | -1.46 | -0.98 | 0.49 |
| | b | 14.46 | 14.61 | 14.06 | 14.06 | 14.30 | 0.28 |
| | R ² | 0.9972 | 0.9946 | 0.9240 | 0.9913 | 0.9768 | 0.0353 |
| 4000 psi | a | -1.03 | -0.53 | -1.25 | -1.18 | -0.99 | 0.33 |
| | b | 15.04 | 14.40 | 15.31 | 14.20 | 14.74 | 0.52 |
| | R ² | 0.9625 | 0.9351 | 0.9270 | 0.9979 | 0.9556 | 0.0320 |
| 5000 psi | a | -0.53 | -0.91 | -1.45 | -1.42 | -1.08 | 0.44 |
| | b | 16.41 | 15.31 | 14.71 | 14.64 | 15.27 | 0.82 |
| | R ² | 0.9709 | 0.9962 | 0.9574 | 0.9925 | 0.9793 | 0.0183 |

The lowermost value of R² is 0.9165, while the lowermost average value is 0.9550. Both values are higher than 0.9, showing that there is a good fitting coefficient for all pressures studied at this work. Thus, this method showed to be suitable as a model for the data analysis of the discrete measurements made in laboratory for the system of oil B and brine B.

4.1.3 Fluid with CO₂

The measurements with CO₂ were carried out with the Model oil II. Figure 21 shows the time dependence of IFT at 1000 psi for this test. In contrast with the other experiments, the R² of this one is 0.7600. However, this low value of R² indicates that it

is least likely a good fitting process for this system (Model oil II + Brine B + CO₂). This should be confirmed through more experiments.

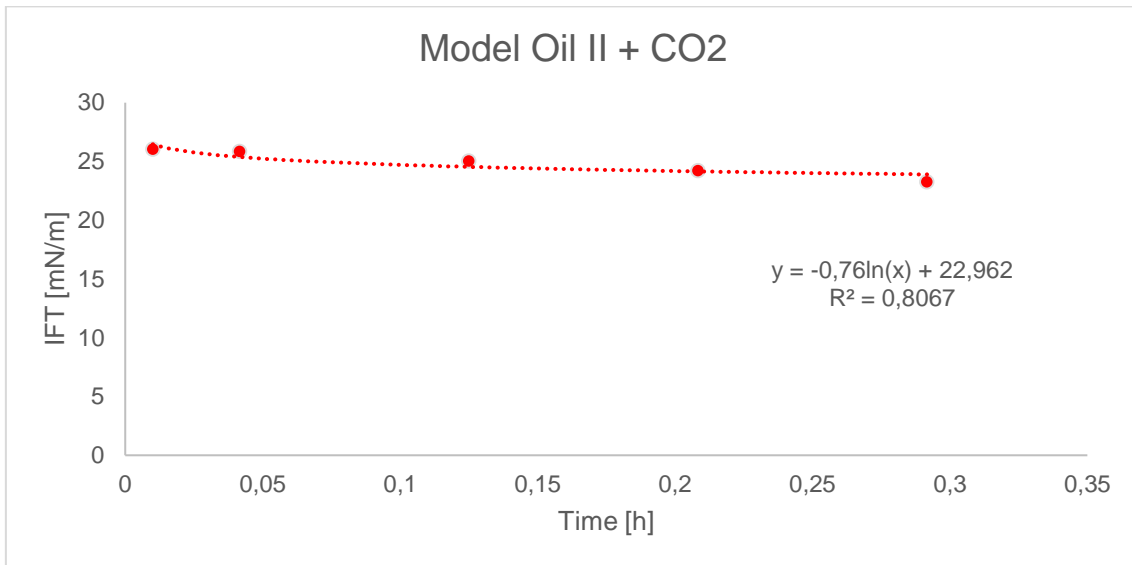


Figure 21 - Experimental IFT of Model Oil II x Brine B with CO₂ at 1000 psi

The time dependence in Figure 22 is different from all others shown in this work so far. Instead of having a negative logarithmic profile, this experiment had a positive behavior, i.e. the IFT value increases with time. The high R² value of 0.998 should indicate a good fit of the data. However, the small amount of points present during the fitting process bias the R² result. For example, it is possible to get a R² = 1 fitting a curve with only 2 points. Thus, even though the R² value is almost 1, it can not be used to take any conclusions.

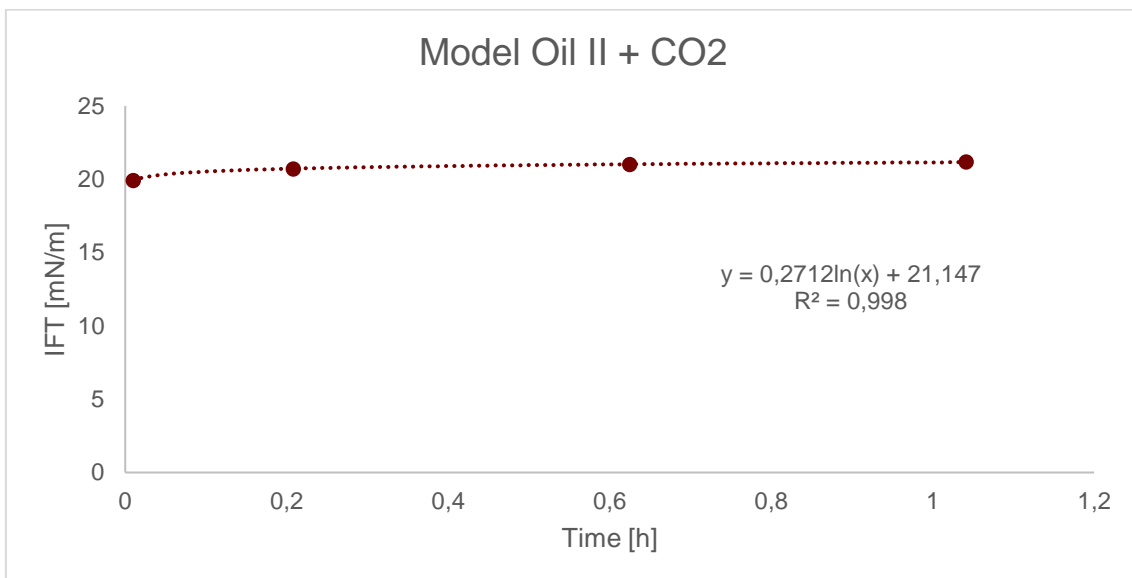


Figure 22 - Experimental IFT of Model Oil II x Brine B with CO₂ at 5000 psi

To sum up, to take accurate conclusions about this system (Model Oil II + Brine B + CO₂), one should run more experiments. However, this fitting process might not represents these experiments as well as it does when there is no CO₂ in the system.

4.2 Stabilization time

From this point, this work considers the fitting function as a reliable modeling method and each test will be represented by its own function. The average value of several similar experiments will be taken as the more correct result. This analysis will be done by applying the concept expressed in page 27, using equation (24).

4.2.1 Fluids without CO₂

4.2.1.1 Model Oil I

Figure 23 can be used to determine the most adequate threshold value for calculating the stabilization time of the experiment. A function derivative of 0.01 mN/mh will give a stabilization time of 249 hours for the 1000 psi experiment and 233 hours for the 5000 psi experiment. However, increasing the threshold to 0.02 mN/m, both values decay drastically to 125 hours and 117 hours, due to the logarithmic modeling. The question is to find at what value the measurement is considered to be stable. By adjusting the threshold value, the resulting error can be altered.

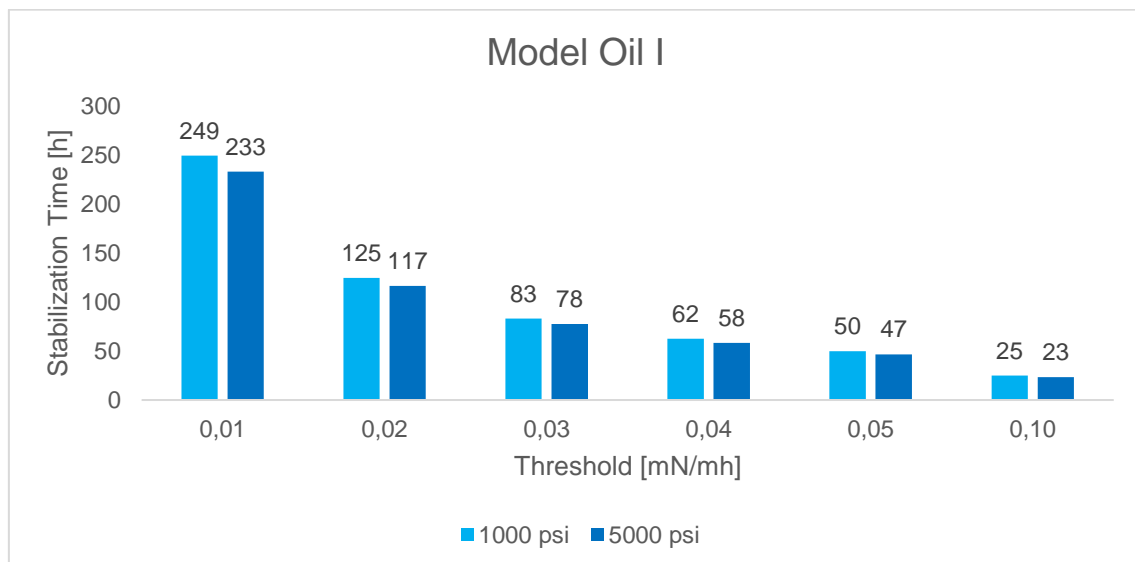


Figure 23 - Stabilization time of Model Oil I with different thresholds

Figure 24 shows the different values of stable IFT calculated as a function of the threshold value. Looking at this bargraph it is possible to notice that the greatest difference in the calculated equilibrium IFT is lower than 6 mN/m for both measurements.

As shown in Figure 4, significant changes in the capillary number require a change of 100 to 1000 times in the IFT. Thus, for this application the threshold value will not affect the obtained results significantly.

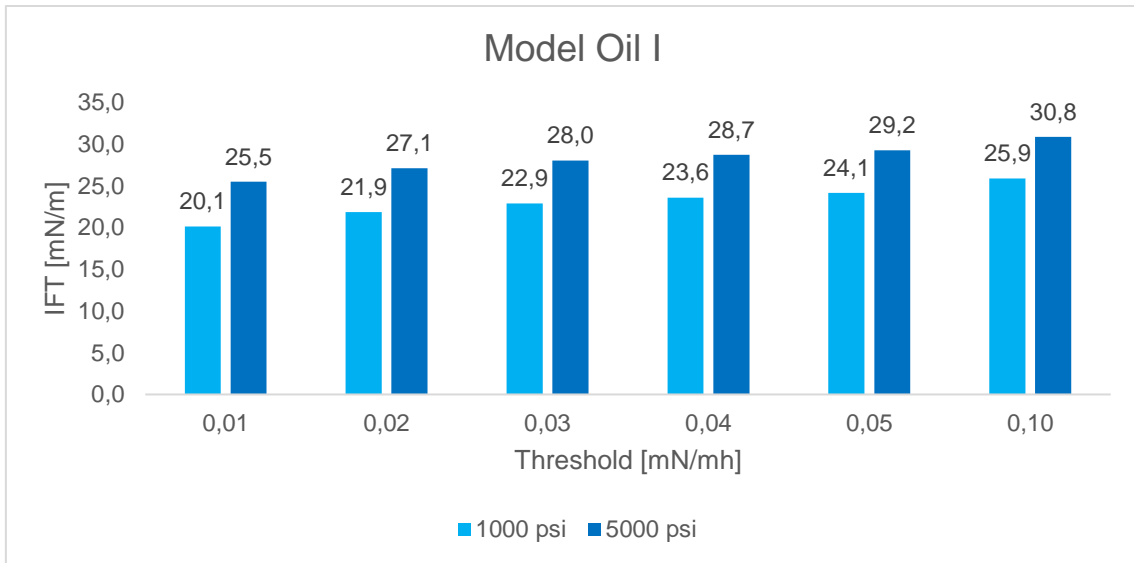


Figure 24 - Model Oil I IFT values for different thresholds

Figure 25 shows a better visualization of the time dependence for this system by a semi-logarithmic plot. Analysing the slope of the curve it is possible to notice that at both pressures the rate of change is almost the same. Another observation is that IFT measurements are higher at higher pressures.

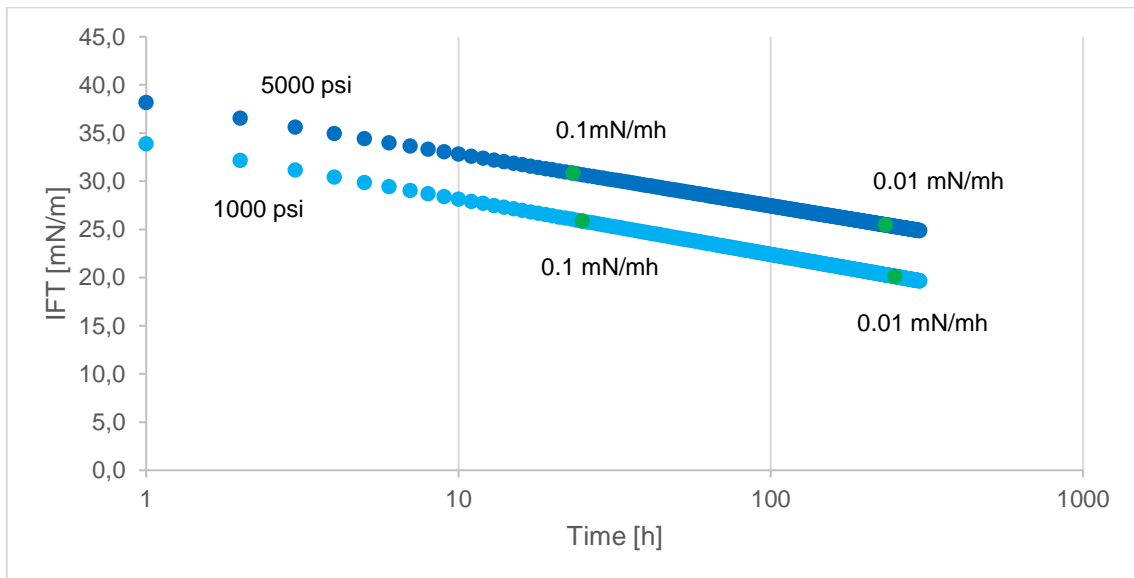


Figure 25 - Semilog plot of model oil I calculated IFT

4.2.1.2 Model Oil II

Figure 26 shows the behavior of the stabilization time as a function of threshold for this system. The plot shows that tests with lower pressure tend to take longer periods to stabilize. This may be due to the increase in the rate of mass transfer at the interface with pressure.

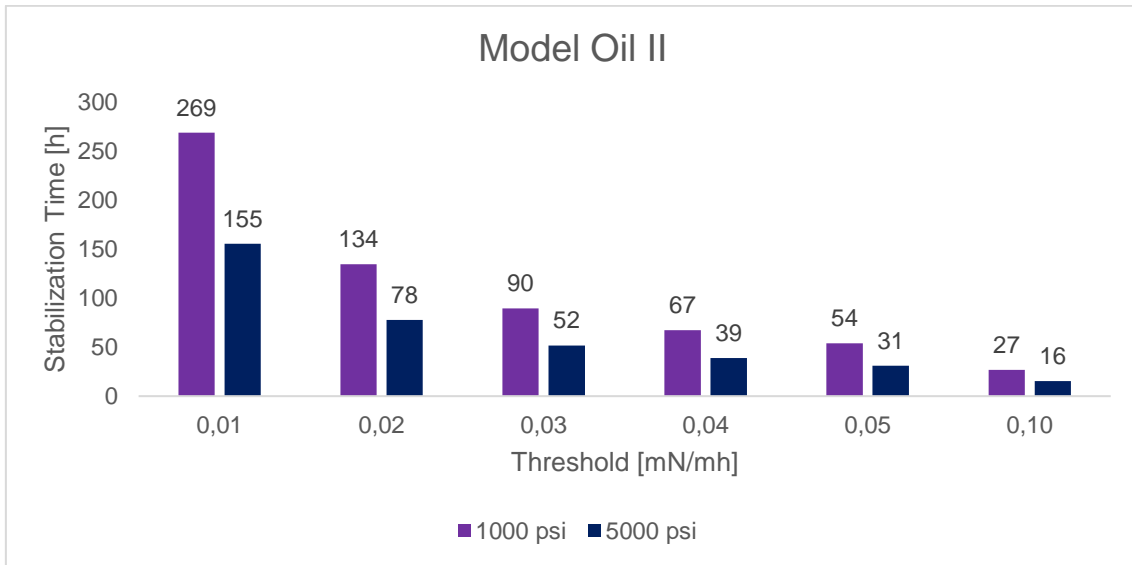


Figure 26 - Stabilization time of Model Oil II with different thresholds

As shown in Figure 27, the threshold has a lower impact if the measurement results in lower stabilization times (i.e. at higher pressures). The difference between the 1000-psi measurement at 0.1 and 0.01 mN/mh is about 6.1 mN/m while the same difference for the 5000-psi experiment is only 3.5 mN/m.

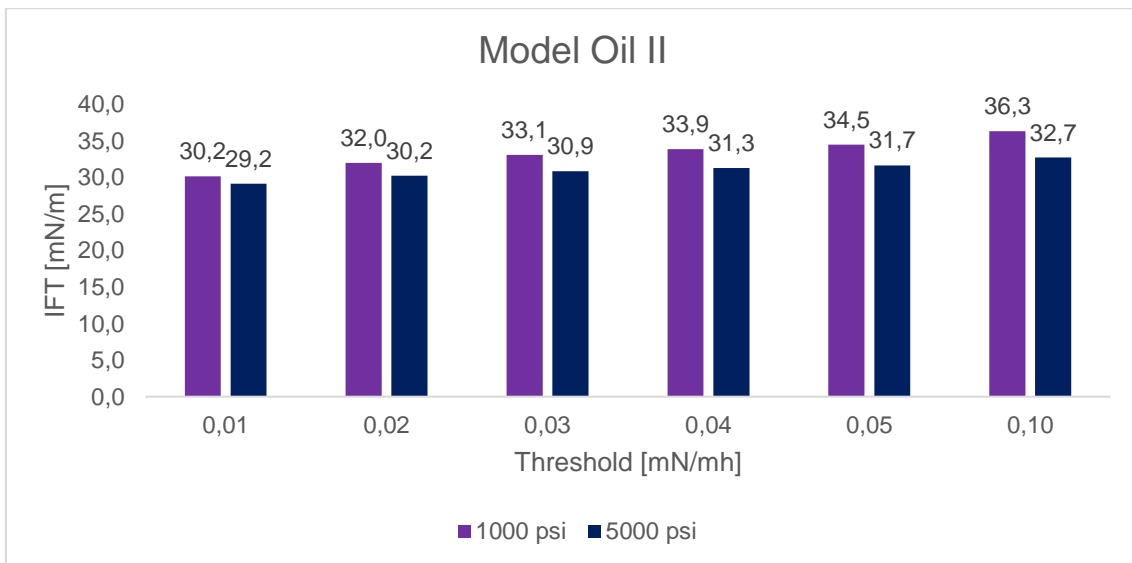


Figure 27 - Model Oil II IFT values for different thresholds

Figure 28 shows the semilog plot of IFT versus time for model oil II. This plot shows that the rate of change at 5000 psi is lower than at 1000 psi. In addition, measurements of 1000 psi are always higher than the other one.

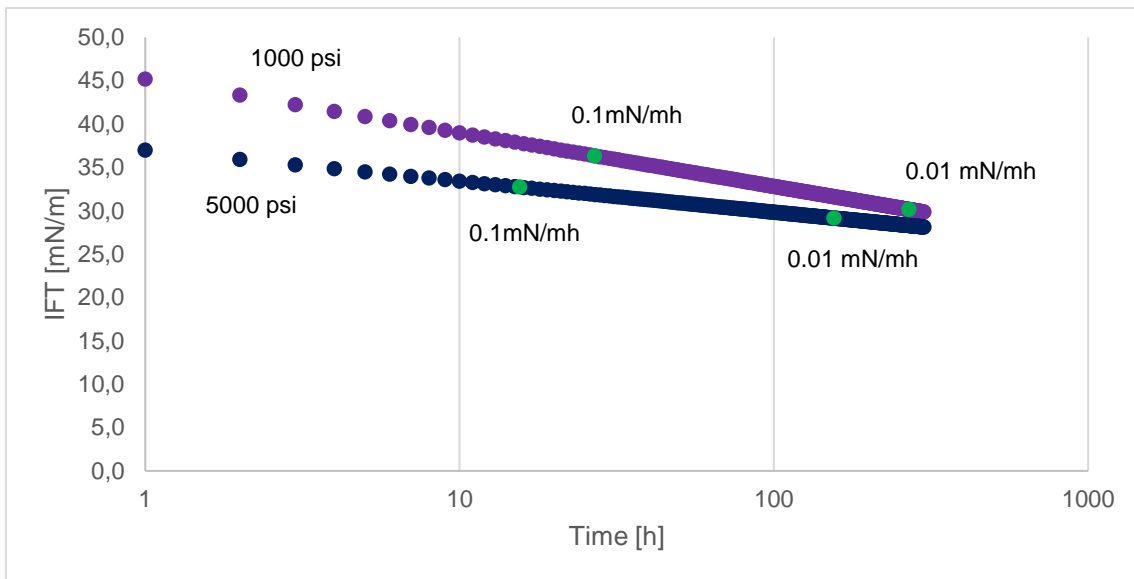


Figure 28 - Semilog plot of model oil II calculated IFT

4.2.1.3 Oil B

The system Oil B + Brine B shows a different behavior regarding rate of stabilization than the previous two systems, as shown in Figure 29. In contrast to the previous results, IFT stabilizes at earlier times for lower pressures. With a larger spectrum of pressures, there is a direct dependence between pressure and stabilization time.

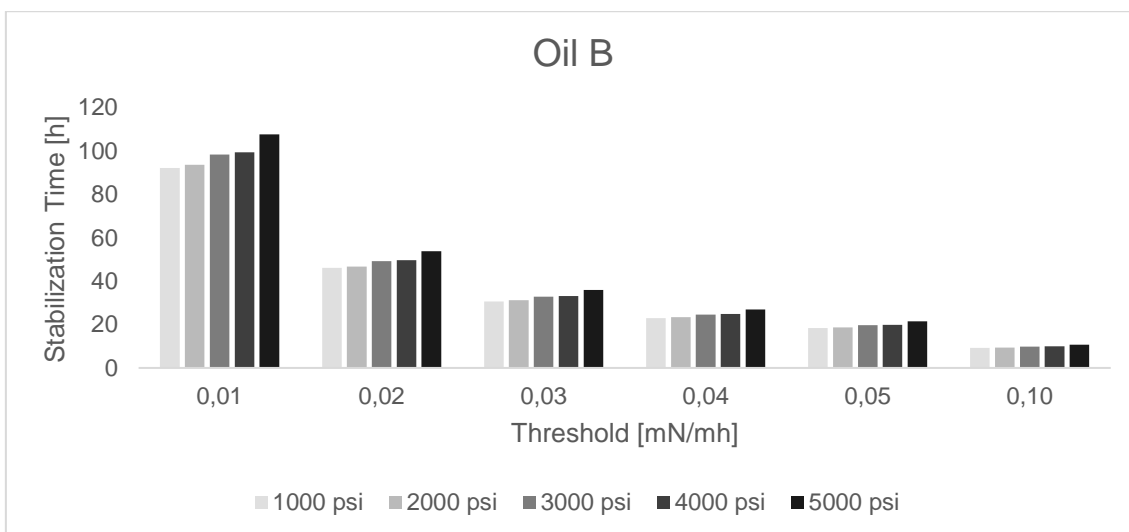


Figure 29 - Stabilization time of Oil B with different thresholds

However, when analysing Figure 30, it is possible to notice that the pressure dependence in IFT measurements for this system are not clear. Actually, within the uncertainty range, all measurements are considered compatible. In addition, the impact of the threshold value is nearly null, because there is no clear difference between the values taken at 0.1 and 0.01 mN/mh.

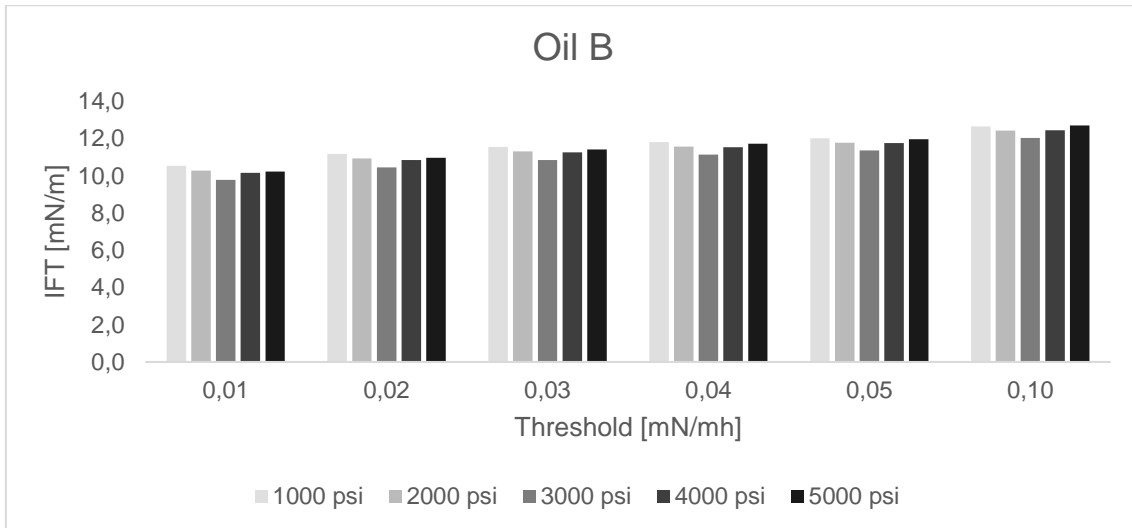


Figure 30 - Oil B IFT values for different thresholds

As the both previous two systems, this one has almost no dependence of the threshold value.

Figure 31 illustrates the time dependence of IFT for oil B at only 1000 and 5000 psi. The other measurements were not plotted because they overlay each other, making it difficult to analyse the chart. It is clear that both measurement are very similar, with the slope of the 1000-psi measurement a little smaller. This corroborates that all the results lie within the same order of magnitude.

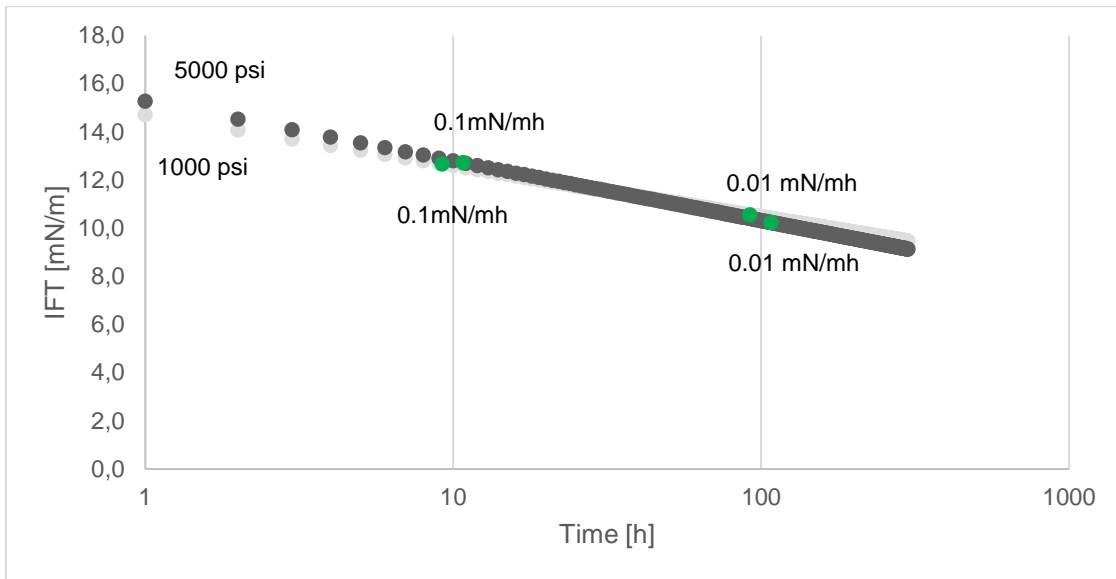


Figure 31 - Semilog plot of Oil B calculated IFT

4.2.2 Fluid with CO₂

Figure 32 shows the stabilization time dependence with threshold value.

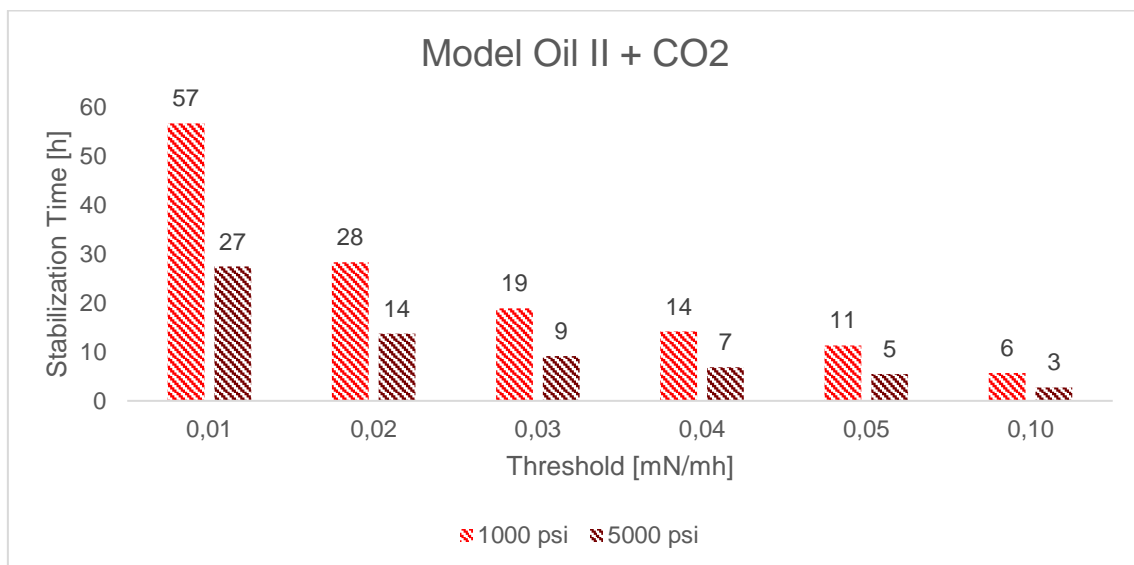


Figure 32 - Stabilization time of Model oil II + CO₂ with different thresholds

This system (Model Oil II + Brine B + CO₂) shows a clear difference with the previous ones. While the system without CO₂ (Model oil B + Brine B) at a threshold of 0.01 takes 269 and 155 hours to stabilize at 1000 and 5000 psi (Figure 26) respectively, this process takes only 57 and 27 hours to achieve an equilibrium at the same conditions when CO₂ is involved. This may indicate that the presence of CO₂ speeds up the mass transfer stabilization process. On the other hand, the CO₂ concentration may hinder the

mass transfer process. Future work should be done to address the CO₂ effect more accurately.

Figure 33 evidences the different behavior between measurements taken at different pressures, as stated before. However, observing the variation in the plot it may be concluded that stabilization occurs at shorter times i.e. lower than 1 hour, as shown in Figure 22.

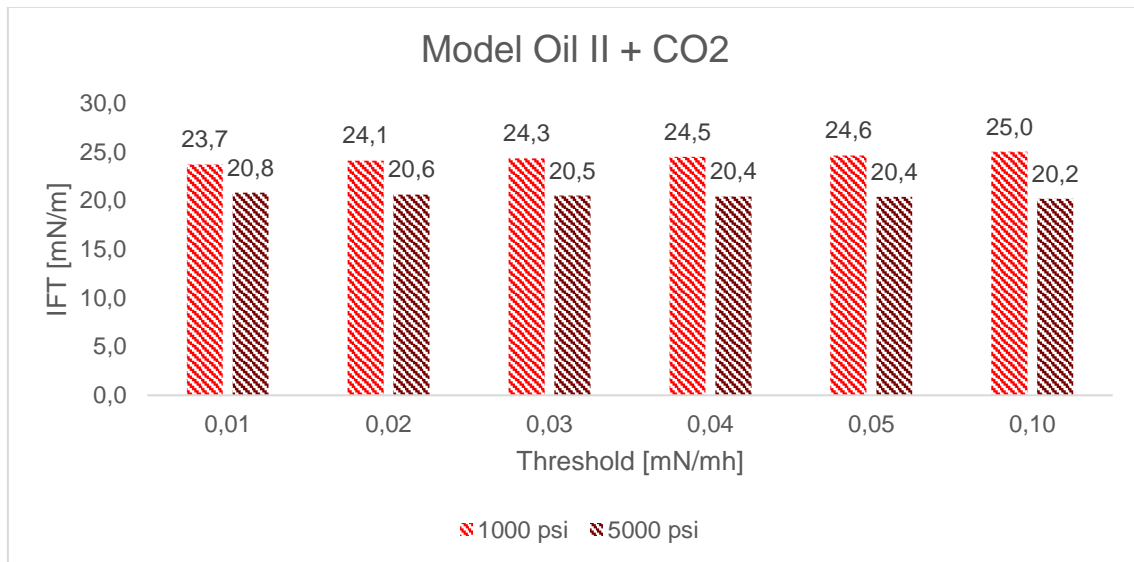


Figure 33 – Model Oil II + CO₂ IFT values for different thresholds

Figure 34 shows a semilog plot of IFT versus time for model oil II with CO₂. It is possible to notice that the slope is positive for the 5000 psi. Also, the stabilization points for this system are at earlier times, if compared to the ones without CO₂. The trend observed in this chart is that at higher pressures, the stabilization process is faster. This may be due to the increase in CO₂ solubility with increasing pressure. Thus, the more CO₂ in the system, the faster the equilibrium IFT will be reached. Another important phenomenon happening is the change of the CO₂ phase to supercritical. As the temperature is above the cricondentherm and the pressure is raised above the cricondenbar, the CO₂ goes to supercritical. This phenomenon alters the behavior of the phases, which could led to different results, as shown.

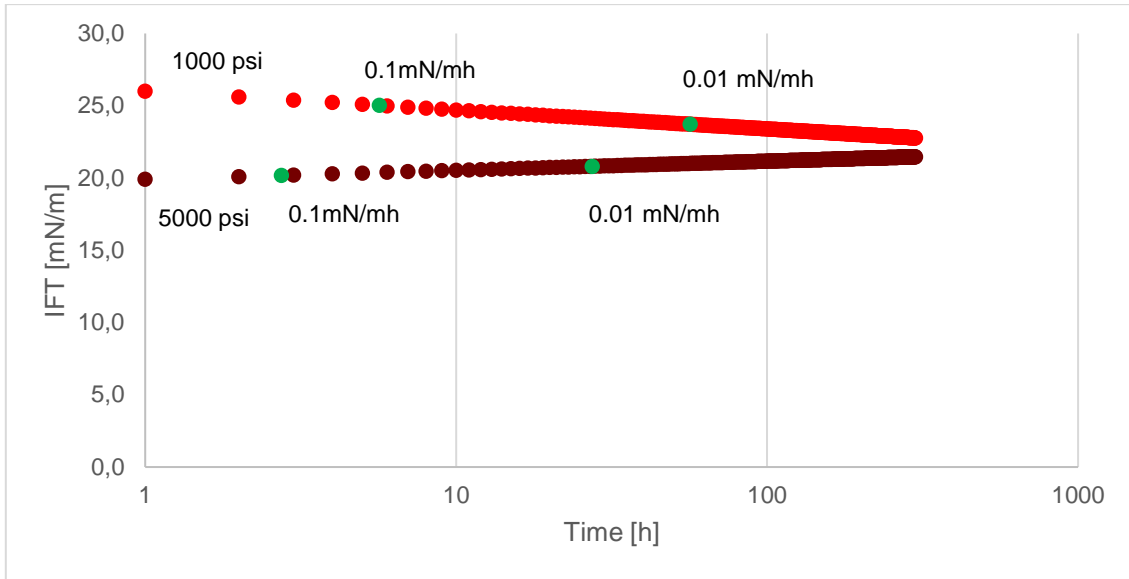


Figure 34 - Semilog plot of Model oil II with CO2 calculated IFT

4.3 Dynamic IFT x Stable IFT

As stated before, the dynamic IFT differs from the equilibrium one. The dynamic IFT stands for the measurements taken at early times of the test, using the average of measurements at 150 and 900 seconds (GEORGIADIS et al., 2011). On the other hand, the stable IFT is the extrapolated value calculated using the logarithmic fitting curve, at the stable time of the measurement. Thus, to standardize the process of calculating the stable IFT, a threshold of 0.01 mN/mh will be used in all systems. Figure 35 illustrates the difference of the shape drop between an early time and a late time measurement.

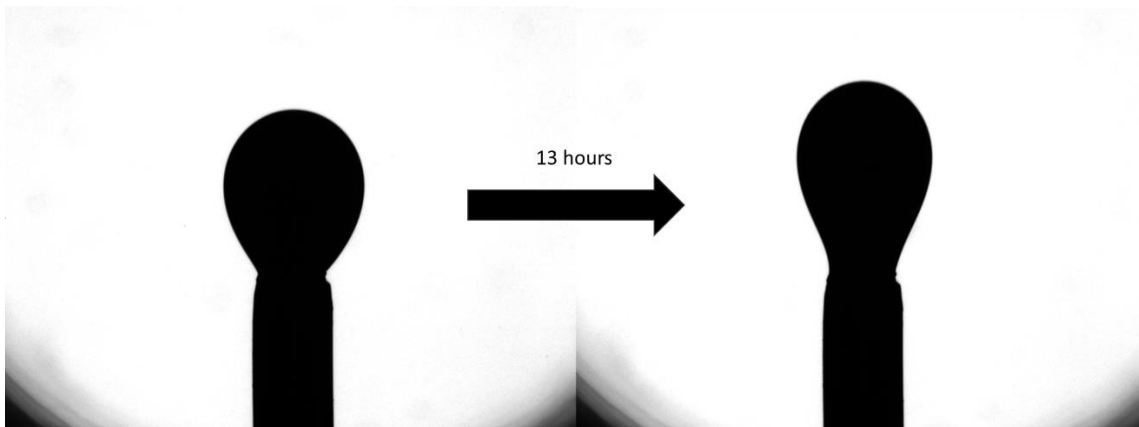


Figure 35 - Time lapse of drop phase (Oil B x Brine B at 5000 psi)

4.3.1 Fluids without CO₂

4.3.1.1 Model Oil I

In Model Oil I, illustrated in Figure 36, the expected tendency of IFT decreasing with time is present. The IFT value showed in the chart is with the error bars, illustrating the possible values that the result could assume, given the uncertainties related to its determination.

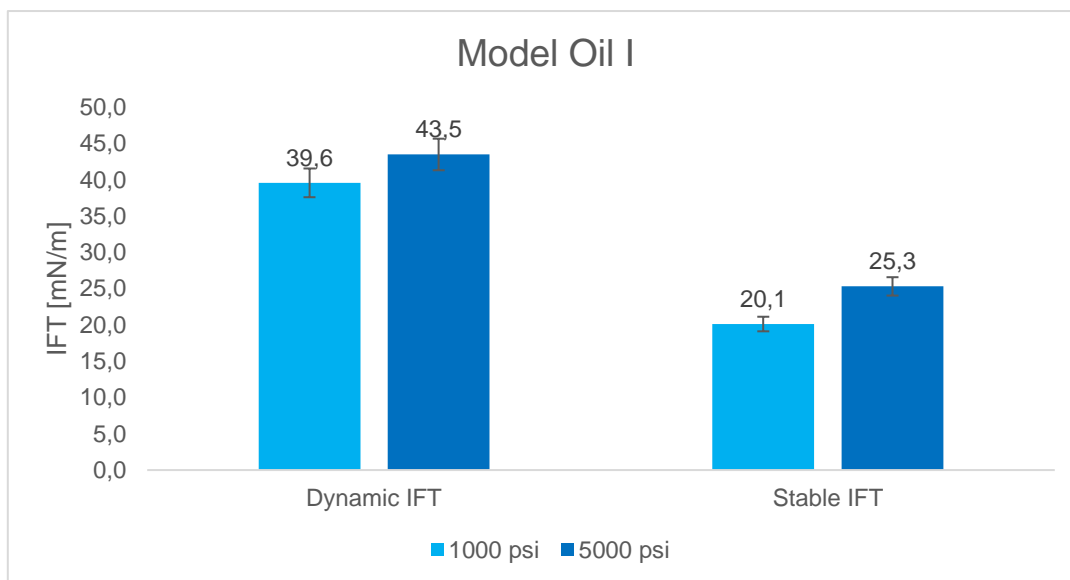


Figure 36 - Model Oil I IFT comparison

The interpretation of the results from Figure 36 are the following:

- Both 1000 and 5000 psi measurements are compatible at dynamic conditions, i.e. given their uncertainty range, they can not be distinguished from each other.
- At stable conditions, the measurements are incompatible, because the error bars do not cross each other. It is possible to say that at 1000 psi, the IFT between Model Oil I and Brine B is lower than the IFT of the same system measured at 5000 psi.
- As Model Oil I is exclusively paraffinic oil (100 wt% n-hexadecane), this high value of IFT at dynamic conditions (about 40 mN/m for 1000 psi) is due to the high immiscibility between both fluids. The alkane phase is composed of apolar molecules while the aqueous phase is composed of polar ones. However, this oil was not purified before the test, so it is possible to have contaminants. With time, these contaminants can migrate to the interface decrease its tension more than the expected. This may be the reason the calculated stable IFT has a smaller value (about 20 mN/m for 1000 psi).

4.3.1.2 Model Oil II

Model Oil II follows the same trends of Model Oil I regarding the comparison between dynamic and stable values for IFT, as shown in Figure 37.

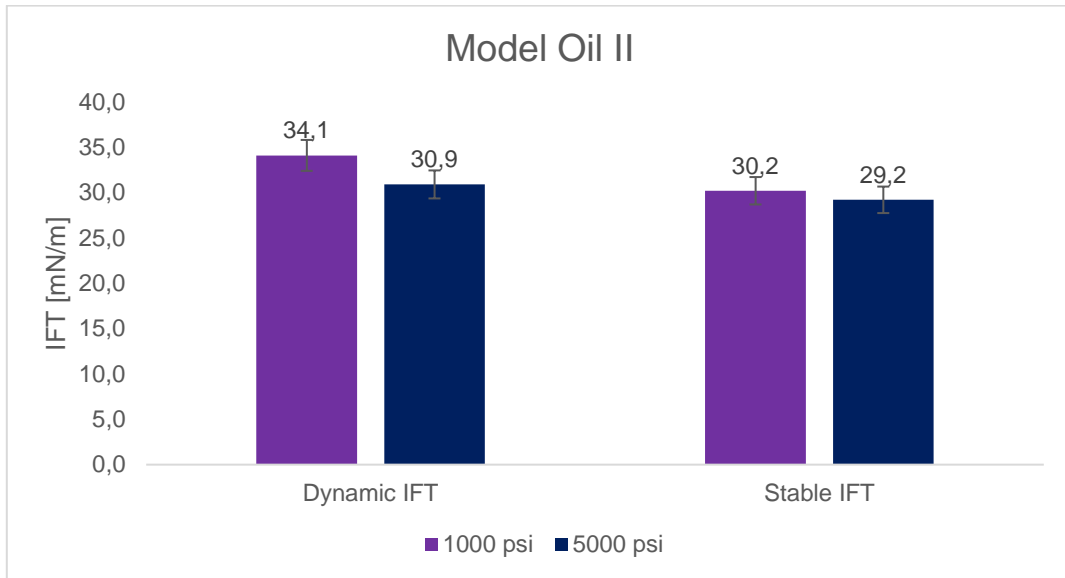


Figure 37 - Model Oil II IFT comparison

Some observations for this system are:

The composition of Model Oil II is n-hexadecane (71.1 wt%) and toluene (28.9 wt%). Both molecules have low dipole moment. Thus, it was expected a high value of IFT, at dynamic conditions, as the previous chart illustrates. Still, both fluids were not purified before the sample preparation. Therefore, the magnitude of the difference between dynamic and stable conditions could have been caused by these impurities.

4.3.1.3 Oil B

The composition of Oil B is shown in terms of SARA analysis at Table 5. The use of a crude oil in this test may bring uncertainties to the analysis due to its complexity. The results illustrated in Figure 38 might be due to the following reasons.

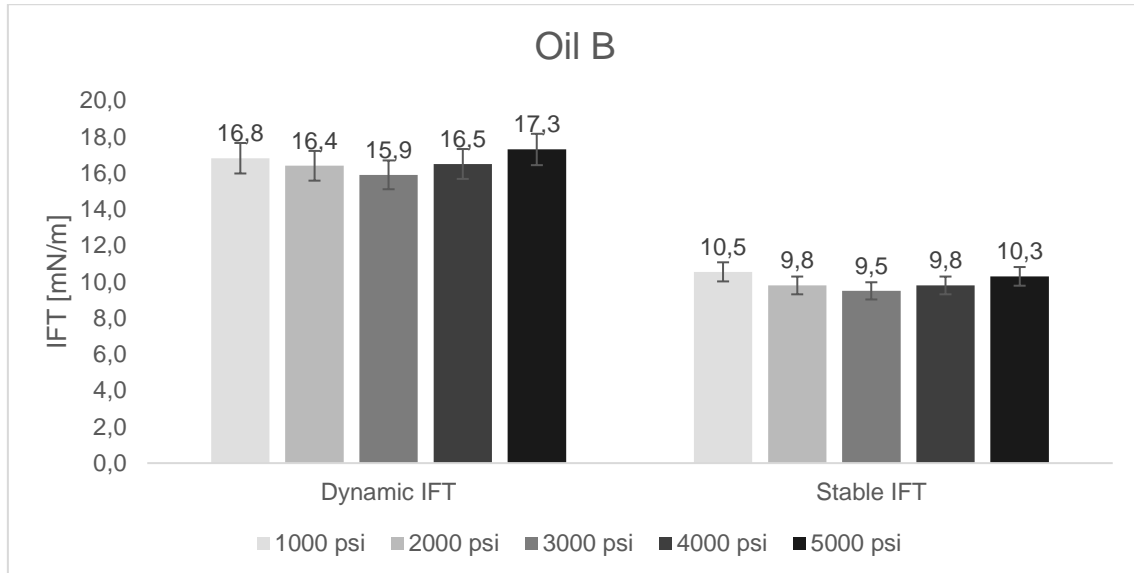


Figure 38 - Oil B IFT comparison

The trend of IFT decaying with time is followed by this system. However, its value does not decay drastically. In addition, the oil phase is rich in resins and asphaltenes (surface-active agents that are not present in the other systems). Both are large molecules that will tend to migrate to the interface because of their amphiphilicity. This migration will result in a low value of IFT, because they act as a surfactant between both phases.

It is important to notice that these results of IFT do not represent the in situ conditions of the reservoir. For these experiments, both oil and brine phases are at dead conditions, i.e. there is no gas dissolved in it. Furthermore, the oily phase does not have its light components, that were at liquid stage at the reservoir conditions, but were evaporated after production.

4.3.2 Fluid with CO₂

The dynamic and equilibrium values for Model Oil II with CO₂ are shown in Figure 39. First, this is the only system in which all measurements are compatible to each other. This is due to the fast stabilization illustrated at the previous topic (page 42).

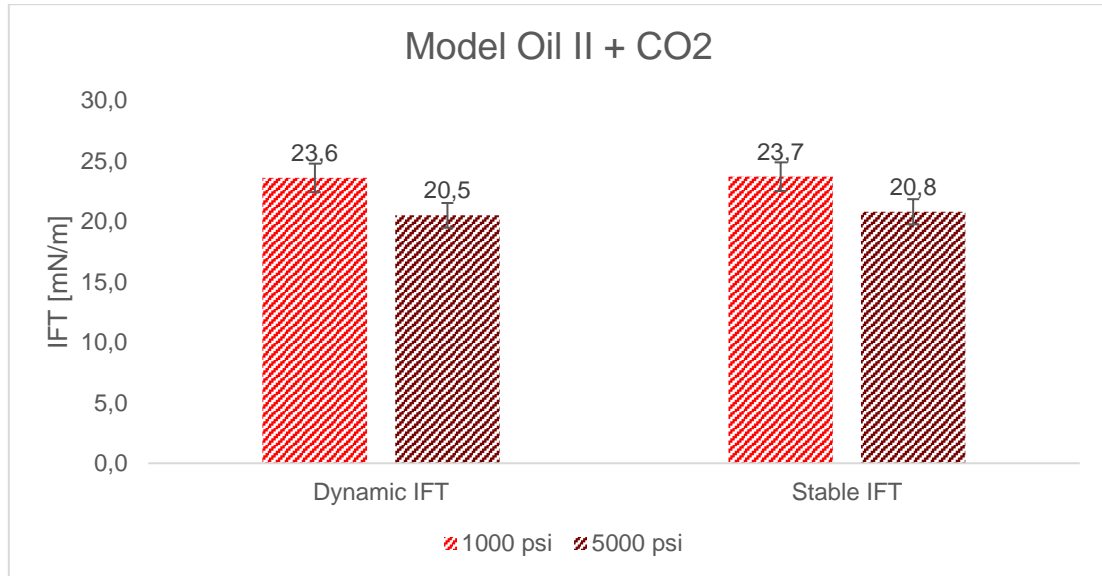


Figure 39 - Model Oil II + CO₂ IFT comparison

4.3.3 Comparison between the systems

Figure 40 shows the IFT comparison for all system without CO₂.

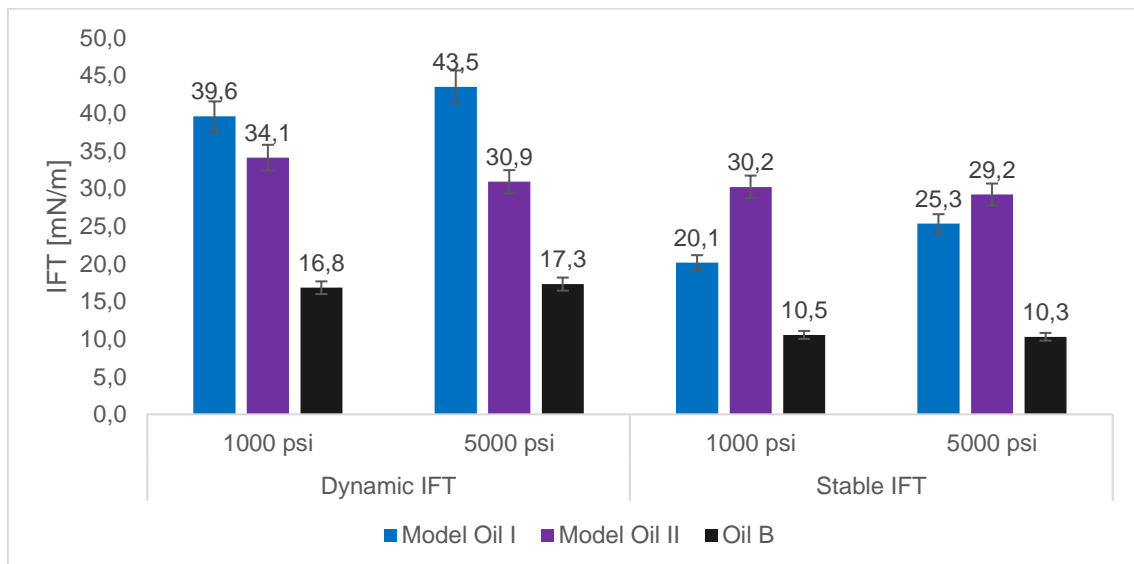


Figure 40 - IFT comparison without CO₂

At low pressure and early time, the interfacial tension of both model oils are among the same order of magnitude. At a higher pressure, this compatibility does not exist anymore. This similarity at 1000 psi might be due to the lack of surface-active

agents in their composition. In addition, it is possible to notice that at early times and 5000 psi, model oil II has a lower IFT value if compared to model oil I. The reason for that is the presence of toluene in model oil II. Toluene has a low dipole momentum. However, when compared to n-hexadecane, toluene is considered a molecule with more polarity. In contrast, at late times, model oil II achieves a high value than model oil I. This may be due to the higher stabilization process for model oil II.

No matter the conditions of pressure or time, oil B has a lower IFT with brine B than both model oils. Maybe due to the presence of resins and asphaltenes, the IFT of the dead crude is always lower than the synthetic oils. In addition, the density difference between Oil B and Brine B is lower than the same difference for both model oils, as Figure 41 shows. As stated before, the IFT is directly proportional to the density difference between both phases.

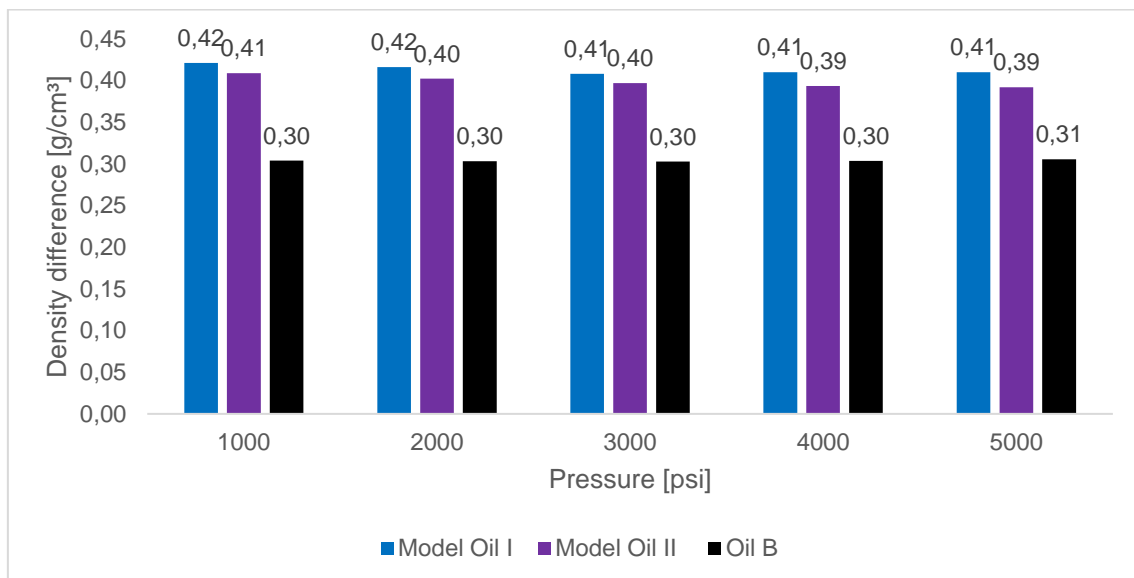


Figure 41 - Density difference between brine and oily phases

Finally, Figure 42 shows the comparison between Model Oil II with and without CO₂. As expected, the presence of CO₂ in the fluids diminished the IFT of the system at dynamic conditions. However, at stable conditions, due to the fast stabilization in the system with dissolved CO₂, the trend is not clear. At 1000 psi, the measurement without CO₂ has a higher value than the other one. At 5000 psi both results are compatible, so it is impossible to define which one is the higher at these conditions. This reduction in IFT is not relevant, regarding field applications. Probably, this is only a side effect of injecting CO₂ in a miscible EOR. A live crude oil should be used in order to better represent the real situation. Furthermore, both results are not reliable, because they were not reproduced. Thus, for more solid conclusions to be taken, more analysis should be done.

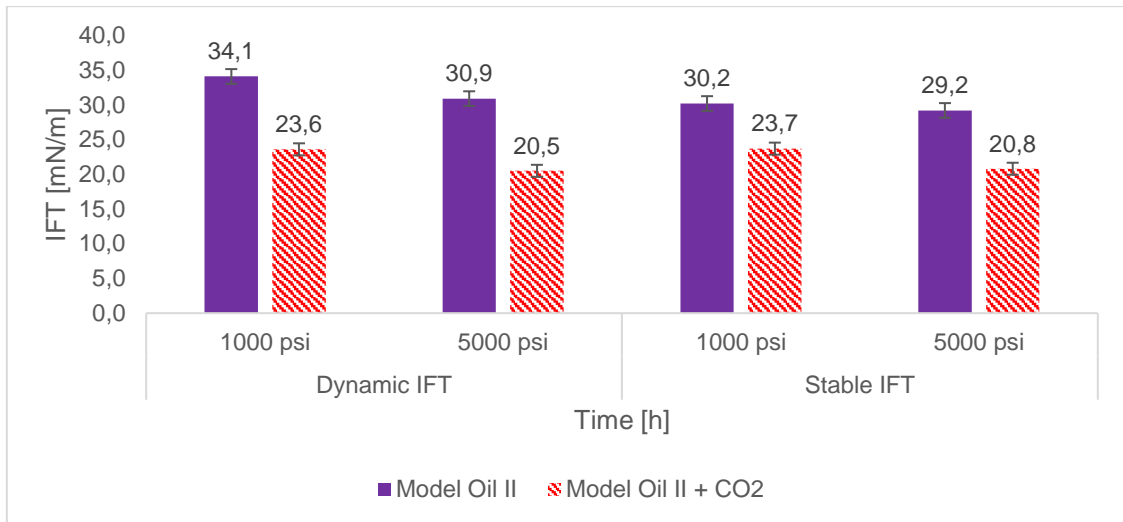


Figure 42 - IFT comparison between Model Oil II with and without CO2

CHAPTER 5: CONCLUSIONS AND FUTURE WORK

The study of interfacial phenomena between fluids is of paramount importance for reservoir engineering. This is an important parameter for EOR techniques, which try to reduce the residual oil saturation at the reservoir. This reduction of residual oil saturation is extremely related to the Recovery Factor, through the volumetric sweep efficiency and the displacement efficiency.

This work studied the interfacial phenomena between fluids at high pressures and temperature. A Pre-salt scenario was addressed by the use of a synthetic formulated brine emulating the real brine of field B. Two model oils were used to understand the contribution of each component in oils that tend to affect fluid-fluid interfaces. In addition, a dead crude oil (from field B, as well) was used.

It was possible to validate the fitting method proposed by this work by testing it in three different systems with dead fluids and one system with dissolved CO₂ in it. System I (Model oil I and Brine B) and system III (Oil B and Brine B) were well modeled by the logarithmic curve and had a minimum R² greater than 0.90. Therefore, with a short period test, it is possible to get a large amount of information. On the other hand, Systems II and IV (Model oil II and Model oil II with CO₂) were experimented only once, thus it was not possible to gather enough information to conclude if they are suitable to this method of modeling.

As it depends on the value of derivative one is assuming to be stable, the stabilization time can assume a wide range of values. However, it does not have a significant impact on the resulting IFT. As the logarithmic function is not asymptotic, at high values of time, the calculated IFT could be near to zero or even negative. Therefore, there must be caution when analysing the stabilization time. In addition, the experiment with CO₂ showed that it has a potential of stabilizing faster.

The difference between dynamic and stable IFT is simply the time moment they are calculated. The dynamic IFT is thought to be free of impurities jeopardizing the experiment. Yet, as the fluids in the reservoir are in contact for geological periods, they are in a stable condition of mass transfer between each other. Thus, it is useful to analyse the two conditions that represent different scenarios.

This work had the goal of validating the method of using a logarithmic fitting function to represent the dynamic data of IFT from DSA experiments. The method was

validated for the systems analysed previously. Therefore, it is now possible to run experiments for fewer hours and achieve reliable results. In consequence, the less time required by the test, the more tests can be run in a range of time.

Future works should address the following topics:

- Reproduction of tests with Model Oil II, in order to validate if the curve-fitting model represents it well.
- Experiments with CO₂ dissolved in Oil B.
- Experiments with other oils and brines.
- A wider range of experiments with pure water in order to consolidate the validity of the method.
- Application of a sensitivity analysis to confirm the best range of averaging
- Study of the impact on the vacuum generated in the piston cell during the test preparation

BIBLIOGRAPHY

ANASTASIADIS, S. H. et al. The determination of interfacial tension by video image processing of pendant fluid drops. **Journal of Colloid And Interface Science**, 1987.

ARMSTRONG, J.; COLLOPY, F. **Causal Forces: Structuring Knowledge for Time-Series Extrapolation**. [s.l: s.n.]. v. 12

AWKINS, C. B. C. AND M. F. H. Applied Reservoir Engineering. **Prentice Hall**, 1959.

BACHU, S.; BRANT BENNION, D. **Interfacial Tension between CO₂, Freshwater, and Brine in the Range of Pressure from (2 to 27) MPa, Temperature from (20 to 125) °C, and Water Salinity from (0 to 334 000) mg·L⁻¹**. [s.l: s.n.]. v. 54

CEZAR, A. S. P. et al. **Subsea Solutions in the Pre-Salt Development Projects**. 2015

DA ROCHA, S. R. P.; HARRISON, K. L.; JOHNSTON, K. P. Effect of Surfactants on the Interfacial Tension and Emulsion Formation between Water and Carbon Dioxide. **Langmuir**, v. 15, n. 2, p. 419–428, 1 jan. 1999.

DE GENNES, P.-G.; BROCHARD-WYART, F.; QUÉRÉ, D. **Capillarity and Wetting Phenomena: drops, pearls, waves**. [s.l: s.n.].

DREXLER, S. et al. **EFFECT OF CO₂ ON DENSITY AND SWELLING FACTOR OF PRE-SALT CRUDE OILS AND FORMATION BRINES AT HIGH TEMPERATURE AND PRESSURE**. Rio Oil & Gas 2018, Rio de Janeiro. **Anais...2018**

DREXLER, S. et al. INVESTIGATION OF THE KEY PARAMETERS AFFECTING WETTABILITY OF A BRAZILIAN PRE-SALT CRUDE OIL AND BRINE ON PURE MINERALS THROUGH STATISTICAL ANALYSIS. **Brazilian Journal of Petroleum and Gas**, 2019.

FOWKES, F. M. ATTRACTIVE FORCES AT INTERFACES. **Industrial & Engineering Chemistry**, 1964.

GEORGIADIS, A. et al. Interfacial Tension Measurements of the (H₂O + CO₂) System at Elevated Pressures and Temperatures. **Journal of Chemical & Engineering Data**, v. 55, n. 10, p. 4168–4175, 14 out. 2010.

GEORGIADIS, A. et al. Interfacial tension measurements of the (H₂O + n -decane + CO₂) ternary system at elevated pressures and temperatures. **Journal of Chemical and Engineering Data**, v. 56, n. 12, p. 4900–4908, 2011.

GOZALPOUR, F.; REN, S. R.; TOHIDI, B. CO₂-EOR and storage in oil reservoirs. **Oil and Gas Science and Technology**, 2005.

GRIGG, R. B.; SVEC, R. **Injectivity Changes and CO₂ Retention for EOR and Sequestration Projects**. 2008

GUDMUNDSSON, J. S. **Flow assurance solids in oil and gas production**. [s.l.: s.n.].

HALLI, S. S.; RAO, K. V. **Advanced Techniques of Population Analysis**. [s.l.] Springer US, 2013.

HAMAKER, H. C. The London-van der Waals attraction between spherical particles. **Physica**, 1937.

HEBACH, A. et al. Interfacial Tension at Elevated Pressures Measurements and Correlations in the Water + Carbon Dioxide System. **Journal of Chemical & Engineering Data**, v. 47, n. 6, p. 1540–1546, 1 nov. 2002.

JHO, C. et al. Effect of pressure on the surface tension of water: Adsorption of hydrocarbon gases and carbon dioxide on water at temperatures between 0 and 50°C. **Journal of Colloid and Interface Science**, v. 65, n. 1, p. 141–154, 1 jun. 1978.

KLUSMAN, R. W. Rate measurements and detection of gas microseepage to the atmosphere from an enhanced oil recovery/sequestration project, Rangely, Colorado, USA. **Applied Geochemistry**, 2003.

LASHKARBOLOOKI, M.; AYATOLLAHI, S. The effects of pH, acidity, asphaltene and resin fraction on crude oil/water interfacial tension. **Journal of Petroleum Science and Engineering**, v. 162, p. 341–347, 2018.

LYON, A. Why are Normal Distributions Normal? **The British Journal for the Philosophy of Science**, v. 65, n. 3, p. 621–649, 2013.

MANRIQUE, E. J. et al. **EOR: Current Status and Opportunities** SPE Improved Oil Recovery Symposium Tulsa, Oklahoma, USA Society of Petroleum Engineers, , 2010. Disponível em: <<https://doi.org/10.2118/130113-MS>>

MASSOUDI, R.; KING, A. D. Effect of pressure on the surface tension of water. Adsorption of low molecular weight gases on water at 25.deg. **The Journal of Physical Chemistry**, v. 78, n. 22, p. 2262–2266, 1 out. 1974.

O'CONNOR, P. D. T. Understanding Statistical Process Control, D. J. Wheeler and D. S. Chambers, Addison-Wesley, 1990. Number of pages: 339. **Quality and Reliability Engineering International**, v. 6, n. 5, p. 386, 1990.

PIZARRO, J. O. DE S. et al. **Optimizing Production of Santos Basin Pre-Salt Fields**

through Sound Reservoir Management Practices OTC Brasil Rio de Janeiro, Brazil Offshore Technology Conference, , 2017. Disponível em: <<https://doi.org/10.4043/27993-MS>>

RAO, D. N.; LEE, J. I. Determination of gas-oil miscibility conditions by interfacial tension measurements. **Journal of Colloid and Interface Science**, 2003.

ROSEN, M. J.; KUNJAPPU, J. T. **Surfactants and Interfacial Phenomena: Fourth Edition**. [s.l: s.n.].

SHAW, D. J. **Introduction to Colloid and Surface Chemistry: Fourth Edition**. [s.l: s.n.].

SHENG, J. **Modern Chemical Enhanced Oil Recovery Theory and Practice**. [s.l: s.n.].

SHOSA, J. D.; SCHRAMM, L. L. Surfactants: Fundamentals and Applications in the Petroleum Industry. **PALAIOS**, 2001.

SONG, B.; SPRINGER, J. Determination of Interfacial Tension from the Profile of a Pendant Drop. **J. Collo. Inter. Sci**, v. 184, p. 64–76, 1996.

SUN, C. Y.; CHEN, G. J. Measurement of interfacial tension for the CO₂ injected crude oil + reservoir water system. **Journal of Chemical and Engineering Data**, v. 50, n. 3, p. 936–938, 2005.

SUSNAR, S. S.; HAMZA, H. A.; NEUMANN, A. W. Pressure dependence of interfacial tension of hydrocarbon-water systems using axisymmetric drop shape analysis. **Colloids and Surfaces A: Physicochemical and Engineering Aspects**, 1994.

TAMBURRI, M. N. et al. A field study of the effects of CO₂ ocean disposal on mobile deep-sea animals. **Marine Chemistry**, 2000.

WIEGAND, G.; FRANCK, E. U. Interfacial tension between water and non-polar fluids up to 473 K and 2800 bar. **Berichte der Bunsengesellschaft/Physical Chemistry Chemical Physics**, 1994.

YANG, D.; GU, Y. Interfacial interactions between crude oil and CO₂ under reservoir conditions. **Petroleum Science and Technology**, v. 23, n. 9–10, p. 1099–1112, 2005.